Preprints.org

Article

Not peer-reviewed version

The Enhanced Wagner-Hagras OLS-BP Hybrid Algorithm for Training IT3 NSFLS-1 for Temperature Prediction in HSM Processes

Gerardo Maximiliano Mendez *, Ismael Lopez Juarez, Maria Aracelia Alcorta Garcia, Dulce Citlalli Martinez Peon, Pascual Noradino Montes Dorantes *

Posted Date: 31 October 2023

doi: 10.20944/preprints202310.2072.v1

Keywords: Interval type-3 fuzzy logic systems; hybrid learning; backpropagation method; orthogonal least square method; general type-2 fuzzy logic systems.

Preprints.org is a free multidiscipline platform providing preprint service that is dedicated to making early versions of research outputs permanently available and citable. Preprints posted at Preprints.org appear in Web of Science, Crossref, Google Scholar, Scilit, Europe PMC.

Copyright: This is an open access article distributed under the Creative Commons Attribution License which permits unrestricted use, distribution, and reproduction in any medium, provided the original work is properly cited.

Preprints (www.preprints.org) | NOT PEER-REVIEWED | Posted: 31 October 2023 doi:10.20944/preprints202310.2072.v1

Disclaimer/Publisher's Note: The statements, opinions, and data contained in all publications are solely those of the individual author(s) and contributor(s) and not of MDPI and/or the editor(s). MDPI and/or the editor(s) disclaim responsibility for any injury to people or property resulting from any ideas, methods, instructions, or products referred to in the content.

Article

The Enhanced Wagner-Hagras OLS-BP Hybrid Algorithm for Training IT3 NSFLS-1 for Temperature Prediction in HSM Processes

Gerardo Maximiliano Méndez [1,*], Ismael López-Juárez [2], María Aracelia Alcorta García [3], Dulce Citlalli Martínez Peón [1] and Pascual Noradino Montes-Dorantes [4,*]

[1] Instituto Tecnológico de Nuevo León-TecNM, Departamento de Ingeniería Eléctrica y Electrónica, Av. Eloy Cavazos 2001, Cd. Guadalupe N. L., México CP 67170. gmm_paper@yahoo.com.mx, gerardo.m@nuevoleon.tecnm.mx. dulce.mp@nuevoleon.tecnm.mx.

[2] CINVESTAV-IPN Saltillo, Robotics and Advanced Manufacturing Department, Ramos, Arizpe, Coahuila, 25900 MX. ismael.lopez@cinvestav.edu.mx.

[3] Universidad Autónoma de Nuevo León, Facultad de Ciencias Físico Matemáticas, San Nicolás de los Garza, N.L., C.P. 66455, México. maria.alcortagr@uanl.edu.mx.

[4] Instituto Tecnológico de Saltillo-TecNM, Departamento de Ciencias Económico-Administrativas, Departamento de educación a distancia, Blvd. Venustiano Carranza, Priv. Tecnológico 2400, Saltillo, Coahuila, México, CP 25280. pascualresearch@gmail.com, pascual.md@saltillo.tecnm.mx.

* Correspondence: GMM gmm_paper@yahoo.com.mx, gerardo.m@nuevoleon.tecnm.mx. +52.81.1624.2893; PNMD pascualresearch@gmail.com, pascual.md@saltillo.tecnm.mx.

Abstract: This paper presents a) the novel hybrid learning method to train the type-1 non-singleton interval type-3 (IT3) fuzzy logic systems (IT3 NSFLS-1) and b) the novel method named enhanced Wagner-Hagras (EWH) IT3 NSFLS-1 fuzzy systems which includes the level *alpha 0* output to calculate the output *y alpha* using the average of the outputs *y alpha k* instead of their weighted average. The development of the proposed methodology uses the orthogonal least square (OLS) method to train the consequent parameters and the back propagation (BP) method to train the antecedent parameters. This proposal dynamically changes the parameters of only the level *alpha 0* minimizing some criterion function as new information becomes available to each level *alpha k*. The antecedent sets are type-2 fuzzy sets, the consequent sets are fuzzy centroids, the inputs are type-1 non-singleton fuzzy numbers with uncertain standard deviations, and the secondary membership functions are modeled as two Gaussians with uncertain standard deviation and the same mean. Based on the firing set of the level *alpha 0*, the proposed methodology calculates each firing set of each level *alpha k* to dynamically construct and update the EWH IT3 NSFLS-1 (OLS-BP) system. The algorithm was tested in a hot strip mill facility to predict the transfer bar surface temperature showing its superior capability to obtain the industrial pyrometer's knowledge uncertainty for tuning and its better performance when compared with IT2 SFLS, IT2 NSFLS-1, GT2 SFLS, GT2 NSFLS-1, IT3 SFLS, and IT3 NSFLS-1 trained with the BP-BP algorithm.

Keywords: interval type-3 fuzzy logic systems; hybrid learning; backpropagation method; orthogonal least square method; general type-2 fuzzy logic systems.

1. Introduction

Interval type-3 (IT3) fuzzy logic systems (FLS) represent a very handy technology according to the state-of the-art literature [1–4], [5–40]. Nowadays, the implementation of IT3 FLS in real life problems is a blank field given the complications presented in this model that is analogous to the general type-2 (GT2) FLS based on the definition in [32]:

Definition 1. *"The type-3 FLS, is the generalization of the type-2 FLS that has more capacity to cope with uncertainties. In T3-FLSs, the secondary membership function (MF) is also a type-2 MF. Then the upper and*

© 2023 by the author(s). Distributed under a Creative Commons CC BY license.

Preprints (www.preprints.org) | NOT PEER-REVIEWED | Posted: 31 October 2023 doi:10.20944/preprints202310.2072.v1

lower bounds of memberships are not constant in contrast to the type-2 MFs. These features cause more levels of uncertainties and can be handled by type-3 MFs. [32, p. 154]"

According to the previous definition and the analogy between the GT2 and IT3 systems, both adhere to the mathematical and methodological principles and to the challenges, difficulties, strengths, and weaknesses that authors defined as complications to face this class of systems [5]. A comprehensive list of challenges to be faced is presented in [41] and are shown in Table 1.

Table 1. Difficulties of GT2 model adapted from [41].

Difficulties	References
Implementation	[42]
Use in practice	[42]
Information is non-functional	[43]
Information is un useful	[43]
Information not needed	[43]
Complex learning process	[44–48]
Hard computation	[44,47–51]
Defuzzification very complex	[44,51,52]
Exhaustive computational time	[44,47–51]
Impractical to usage	[44]
Method iterative and algorithmic	[53]
Determination of the number of levels-α_k	[49]

A brief survey of the state-of-the-art literature shows that the found applications are only from the theoretical point of view of singleton (IT3 SFLS) [3,6–29,31–40] and of type-1 non-singleton (IT3 NSFLS-1) FLS [5, 28 and 29]. This technology presents some challenges and complications in the design and implementation processes. i.e., in [28] the development of a new flowmeter fault detection approach based on optimized non-singleton type-3 (NT3) FLS with type-1 non-singleton inputs is presented. The introduced method is implemented on an experimental gas industry plant. The system is modeled as NT3 FLS system, and the faults are detected by the comparison of measured and estimated signals. According to the authors, the level of non-singleton fuzzification and membership parameters are tuned by a maximum correntropy (MC) unscented Kalman filter (KF), and the rule parameters are learned by correntropy KF (CKF) with fuzzy kernel size.

In contrast to the recent developments on automata's, drones, automated remote vehicles (ARV's) among others, require adaptation, learning, tuning to get the necessary knowledge for adaptation to the changing environments, the applications of IT3 are limited and their analogy with GT2 systems exists as it is documented in [5], e.g., the GT2 NSFLS-1 is used as a controller for control and balance a two-wheel mobile robot [54]. The GT2 NSFLS-1 model is used in a proportional, integral, and derivative (PID) controller to get effectiveness and robustness in a plan controller affected by external disturbances [55].

The GT2 NSFLS-1 model is used to manage efficient and energy conserving permanent magnetic drive [56]. In [57] the GT2 NSFLS-1 is proposed to test and to provide a theoretical framework using the enhanced Karnik-Mendel Algorithm and the Nie-Tan algorithm to see their accuracy. In [58] it is presented an adaptive GT2 non-singleton fuzzy neural network control for motion balance adjusting of a power-line inspection robot. In [59] are presented GT2 NSFLS-1 classifiers for medical diagnosis. A medical application to regulate glucose levels is proposed in [60]. In [61] it is presented a model to synchronize chaotic systems affected by external disturbances.

The difficulties presented in Table 1 happen in the GT2 and IT3 singleton fuzzy systems in both, Mandami and Takagi-Sugeno-Kang (TSK) models, and it is remarkable that happens in the singleton form that is the simplest or primitive form of fuzzy systems, in [41–45,47–51,60–90] for GT2 FLS and

Preprints (www.preprints.org) | NOT PEER-REVIEWED | Posted: 31 October 2023 doi:10.20944/preprints202310.2072.v1

[91–117] IT3 FLS. In contrast for the case of the IT3 type-1 non-singleton systems there are only a limited number of applications [19, 20, 29 and 40] and for IT3 type-2 non-singleton there is only one, [5]. In the state-of-the-art modern literature, the reference to IT3 NSFLS-1 and to IT3 NSFLS-2 is practically inexistent but in contrast the synonym (generalized type-2 non-singleton) used for this technology of knowledge acquisition for tuning, adaptation, updating, learning, or training shows that from 2021 until now there are 44 papers that include proposals with type-3 fuzzy logic systems. There are 39 publications named as "shadowed type-2" fuzzy systems. Using the "knowledge acquisition" there are 10 papers with learning, 8 papers with tuning, 11 papers for adaptation and only four papers for updating, as shown on Table 2. Table 3 shows the literature on IT3 FLS in their singleton and non-singleton versions with 52 papers of type-3 fuzzy logic systems. For knowledge acquisition there are 4 papers with hybrid learning, 38 papers with learning, and 33 papers with tuning, 30 papers for adaptation and only 5 papers for updating, one or more of these terms are mentioned in the same paper.

Table 2. Survey of techniques used to train the GT2 FLS models.

R	GT2		Optimization model	Knowledge acquisition Designation				System designation		
	S	N		L	T	A	U	GT2	Generalized type-2	Shadowed type-2
[15]		X	TW, robustness analysis		X					X
[44]	X		Ordered weighted averaging (OWA)	X			X	X		
[45]	X		Data-driven			X		X		
[47]			Kalman Filters	X		X		X		
[48]	X		Artificial Neural Networks			X		X		
[52]	X		Recursive Least Squares (RLS), Gradient-based Method, hybrid ANN to optimize clustering	X				X		
[55]		X	Social spider optimization				X	X		
[58]			Particle Swarm Optimization (PSO)			X		X		
[60]	X		Biogeography-Based Optimization (BBO)	X				X		
[64]	X		Least Square Estimator (LSE), Teaching Learning Based Optimization (TLBO)			X		X		
[72]			Searching algorithms	X	X			X		
[73]	X	X	Ant lion optimizer				X	X		X
[79]	X		Hybrid Differential Evolution Algorithm			X		X		
[82]		X	Harmony search			X			X	X

Preprints (www.preprints.org) | NOT PEER-REVIEWED | Posted: 31 October 2023 doi:10.20944/preprints202310.2072.v1

[83]	X	SVM, Decision trees, ANN, Bagging and boosting, bagging, boosting, GD, fuzzy entropy, PSO,	X	X	X	X				X	
[84]	X	Backpropagation algorithms and RLS	X		X			X			
[85]	X	Lyapunov function	X	X	X		X	X			
[86]	X	Kernel ridge regression (KRR)	X					X			
[87]	X	Hierarchically stacked though, gradient descent (GD), gaussian kernel, support vector machine (GSVM)	X	X	X			X			
[88]	X	Multi-objective optimization.	X				X				
[90]	X	Tuning laws (TW)	X	X	X		X				

R is the reference number, GT2 is for General type 2 system, S is singleton, N is non-singleton type-1, L for learning, T for tuning, A for adaptation, and U for Updating.

Table 3. IT3 FLS systems.

Ref.	**IT3 System**			**Learning Algorithm**	**Knowledge acquisition designation**				
	S	**N-1**	**N-2**		**Hybrid**	**L**	**A**	**U**	**T**
[1]	X			Classification system does not show a learning algorithm or does not need it		X	X		X
[2]	X			Theoretical proposal for modelling and compare the IT3 and IT2 systems do not show the use of learning	X	X	X		X
[4]	X			Differential evolution		X	X		X
[5]			X	Gradient descend	X	X	X	X	X
[7]	X			Empirical knowledge of experts combined with a trial-and-error approach		X	X		X
[8]	X			Fractal dimensions		X	X		X
[9]	X			Statistical measures, fuzzy c-means clustering and granular computing using to construct the model not for learning				X	
[11]	X			Response aggregation		X	X		X
[12]	X			Backpropagation with momentum learning		X	X		X

Preprints (www.preprints.org) | NOT PEER-REVIEWED | Posted: 31 October 2023 doi:10.20944/preprints202310.2072.v1

[13]	X		Specific adaptation law		X	X		X
[14]	X		Fractional-order model based on restricted Boltzmann machine (RBM) and deep learning contrastive divergence (CD)		X			X
[15]	X		Pitch adjustment rate (PArate) parameter in the original harmony search algorithm (HS)		X			X
[18]		X	Upper bound of approximate error (AE)					
[19]		X	Fractional order		X			X
[22]	X		Fuzzy c-regression model clustering algorithm			X		X
[25]	X		Deep reinforcement learning (DRL)		X			X
[26]	X		Unscented Kalman filter (CUKF)	X	X	X	X	X
[27]	X		Surge-guided line-of-sight (SGLOS) and auxiliary dynamics		X	X		X
[28]		X	Maximum correntropy (MC) Unscented Kalman filter (UKF)		X	X		X
[33]	X		Specific control law		X			
[39]	X		Kalman filter (UKF)		X			
[40]		X	Lyapunov adaptation rules			X		X
[92]	X		Hybrid Learning ARIMA LSTM LSTM	X	X			
[93]	X		Robust adaptive command-filtered backstepping control scheme, adaptive laws	X	X			
[94]	X		This is a survey, not a theoretical paper and not an application or development		X	X		X
[96]	X		Bacterial foraging optimization algorithm		X			X
[97]	X		Do not have learning is a classification model		X			X
[98]	X		Spherical Fuzzy MARCOS MCGDM		X			X
[99]	X		Weighted least square (WLS)					X
[100]	X		Actor-critic learning control algorithm and associated with Lyapunov stability examination		X	X		X
[101]	X		+Nonlinear model predictive control (NMPC)		X			X
[102]	X		+Marine predator		X	X	X	X
[103]	X		+Maximum power point tracking (MPPT), genetic algorithm					X
[104]	X		+Differential evolution			X		X

Preprints (www.preprints.org) | NOT PEER-REVIEWED | Posted: 31 October 2023 doi:10.20944/preprints202310.2072.v1

[105]	X	+Harmony search		X	X	
[106]	X	+Harmony search and the differential evolution		X	X	
[107]	X	Not learning algorithm, the parameters are changed manually		X	X	
[108]	X	Terminal sliding mode controller		X	X	
[109]	X	Adaptive sliding mode disturbance observer, adaptive laws, an output with continuous-time linear systems.	X	X	X	
[110]	X	Retained region approach (granulation)		X	X	
[111]	X	Multi-objective Artificial Hummingbird Algorithm (MOAHA)		X		X
[112]	X	Enhanced Kalman filter (EKF)				X
[113]	X	*Survey of methods is not an application		X		
[114]	X	Extended state space model-based constrained predictive functional control		X		
[115]	X	+ Event-triggered control law		X		
[116]	X	+ Cartograms to visualize both the expansion and spread		X		
[117]	X	+ Non-linear time series		X		

S for singleton, N-1 for non-singleton 1, N-2 for non-singleton 2, L for learning, T for tuning, A for adaptation, and U for updating; + the learning algorithm is only used to obtain the information for the rule base or for optimization.

The few applications found in the state-of-the-art literature, the difficulties in optimizing the models, the fact of multiple calculation to obtain several numbers of planes as mentioned in [83] and the requirement of iterative methods to train the model have led researchers to use different models which stand out principally in GT2 SFLS systems for acquiring knowledge, learning, and tuning in their different definitions.

To the best of the authors' knowledge, studies of GT2 NSFLS-1 and IT3 NSFLS-1 that use the OLS-BP hybrid learning mechanism as a training method have not been found in the state-of-the-art literature. However, there are publications presented elsewhere referring to the IT2 Mamdani FLS [118–121], and to the IT2 TSK FLS [122,123] using the proposed hybrid OLS-BP mechanism.

As mentioned earlier, the intention of this article is to present and discuss the proposed OLS-BP hybrid learning algorithm for antecedent and consequent parameter tuning of the novel Enhanced Wagner-Hagras (EWH) IT3 NSFLS-1 system and demonstrate its implementation in a real industrial hot strip mill (HSM) application. To enable direct comparison of the performance and functionality of the proposed hybrid mechanism, the same input-output data set is used as in [118–123] and it has been experimentally examined under the same conditions as in previous work.

The main contributions of this proposal are:

1. The detailed mathematical formulation of the hybrid OLS-BP training method using a) the partial derivatives with respect to a performance criterion to tune each parameter for only the antecedent section of the level-α_0 and b) the orthogonal transformations of rotation or OLS method to tune only the consequent parameters of the level-α_0 of the proposed enhanced WH system. This system is named as hybrid enhanced EWH IT3 NSFLS-1 (OLS-BP) fuzzy system.

2. A more precise and economical method to estimate the final value y_α using the simply average of the outputs y_{α_k} of the EWH IT3 NSFLS-1 (OLS-BP) fuzzy system, which includes the

Preprints (www.preprints.org) | NOT PEER-REVIEWED | Posted: 31 October 2023 doi:10.20944/preprints202310.2072.v1

horizontal level-α_0 or IT2α_0 FLS output, y_{α_0}, calculated as $y_\alpha = \frac{\sum_{k=0}^{N} y_{\alpha_k}}{N+1}$, instead of the classic WH method using the weighted average: $y_\alpha = \frac{\sum_{k=1}^{k_{max}} \alpha_k y_{\alpha_k}}{\sum_{k=1}^{k_{max}} \alpha_k}$.

3. The use of the alternative method to construct the EWH IT3 NSFLS-1 system with dynamical structure, where each of its N horizontal levels-α_k has its own base of M rules. The output y_{α_k} of each level-α_k is calculated using the antecedent's firing interval $\left[\underline{f}^i_{l\alpha_k}, \overline{f}^i_{r\alpha_k}\right]$ and the consequent's centroid $\left[\underline{c}^i_{l\alpha_k}, \overline{c}^i_{r\alpha_k}\right]$ of each ith rule. According to the WH method for the construction of the EWH IT3 NSFLS-1 system, [5], each output y_{α_k} of each level-α_k is calculated using the estimation of the α_k-cuts at level-α_k. The present proposal does not estimate each α_k-cut of each input x'_q at each level-α_k, that is the $\left[a^i_{q\alpha_k}(x'_q), b^i_{q\alpha_k}(x'_q)\right]$ interval values, in order to calculate the firing interval values $\left[\underline{f}^i_{l\alpha_k}, \overline{f}^i_{r\alpha_k}\right]$ of this level-α_k. This proposal estimates both, the antecedent firing levels $\left[\underline{f}^i_{l\alpha_k}, \overline{f}^i_{r\alpha_k}\right]$ and the consequent centroids $\left[\underline{c}^i_{l\alpha_k}, \overline{c}^i_{r\alpha_k}\right]$ using a Gaussian models as a secondary membership functions.

4. To the best knowledge of the authors, this is the first time that the hybrid EWH IT3 NSFLS-1 (OLS-BP) fuzzy system is applied to predict the transfer bar surface temperature at the entry zone of the finishing scale breaker of a HSM.

This work is organized as follows. In section 2 the foundations of the proposed EWH IT3 FLS systems, the BP, and the OLS training methods are exposed to let the reader contextualize the proposal also presented in this section. Section 3 presents the application and validation of the performance of the proposed methodology applied to the temperature prediction of the transfer table of the host strip mill facility. Section 4 presents the results analysis obtained in the application. Finally, section 5 provides the conclusions.

2. Materials and Methods

2.1. A new Construction and Calculation of the WH IT3 NSFLS-1 System

The main foundation of IT3 systems is the uncertainty presented by the horizontal level-α_k with respect to its vertical location or its secondary membership value $\mu_{\tilde{A}}(x,u) = f_x(u) = \alpha_k$, as is shown in Figure 1 and Figure 2. In the IT3 systems, this additional uncertainty is represented by the interval value $\left[\underline{\alpha}_k, \overline{\alpha}_k\right]$. Geometrically as in [124], it is interpreted as shown in Figure 3. This uncertainty is modeled to be between the horizontal levels- $\underline{\alpha}_k$ and $\overline{\alpha}_k$, as in Figure 4.

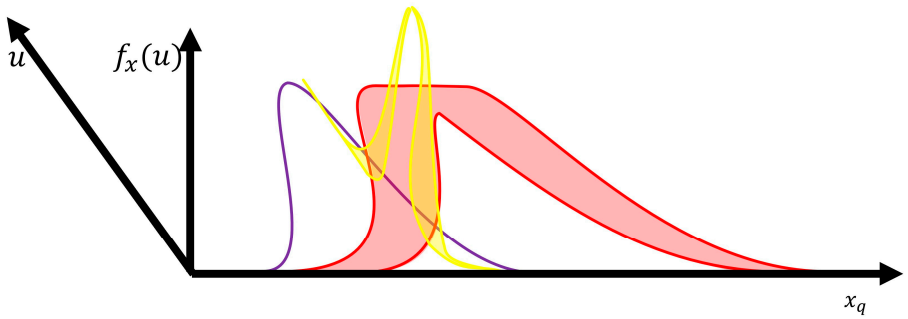

Figure 1. Geometrical view of the GT2 NSFLS-1.

Preprints (www.preprints.org) | NOT PEER-REVIEWED | Posted: 31 October 2023 doi:10.20944/preprints202310.2072.v1

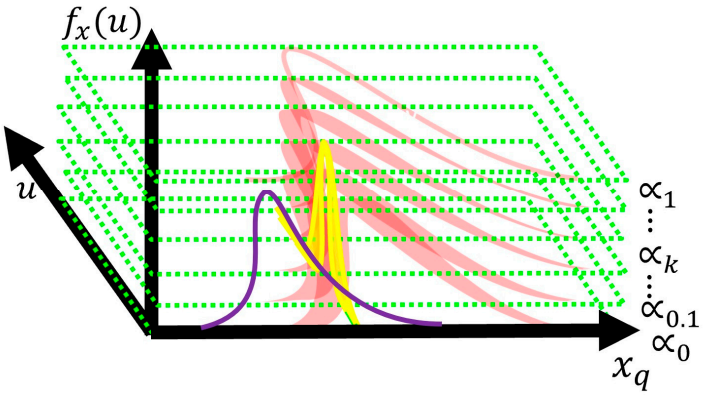

Figure 2. Levels-$\boldsymbol{\alpha_k}$ and uncertain secondary values of the proposed EWH IT3 NSFLS-1 system.

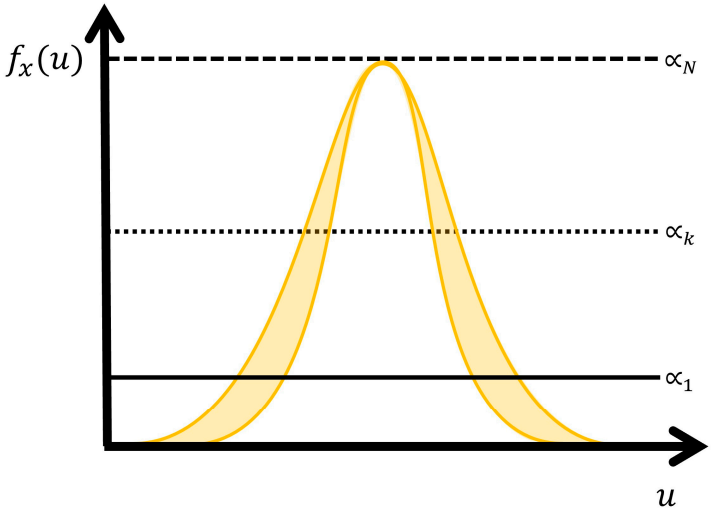

Figure 3. Uncertainty of secondary membership grade in EWH IT3 system.

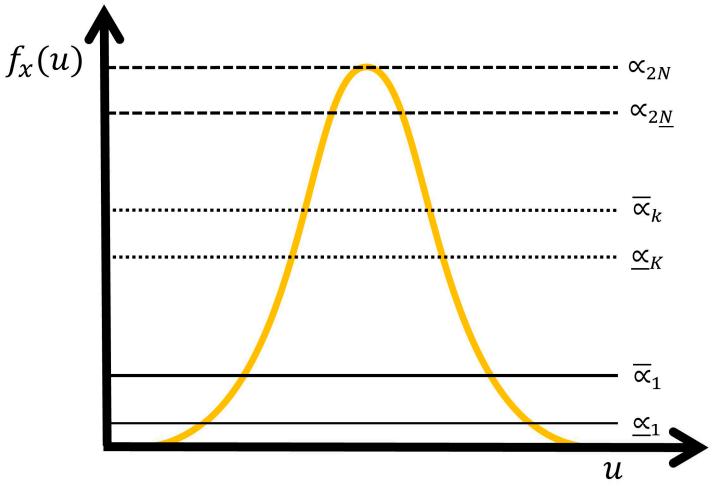

Figure 4. Uncertainty of secondary membership grade in EWH GT2 equivalent to EWH IT3 systems.

Preprints (www.preprints.org) | NOT PEER-REVIEWED | Posted: 31 October 2023 doi:10.20944/preprints202310.2072.v1

Based on the modeling of WH GT2 Mamdani fuzzy systems that use the type reduction center sets and the end-point defuzzification average, [124], Eq. (1), the WH IT3 NSFLS-1 can be calculated in more economical and precise results using Eq. (2), with $q = 1, 2, \dots, p$ the number of input variables, $i = 1, 2, \dots, M$ the number of rules, and $k = 1, 2, \dots, N$ the number of the horizontal levels-α_k.

The classic WH GT2 Mamdani model uses the weighted average of the contribution of each level:

$$f_{WH\ IT3\ NSFLS-1}(\boldsymbol{x}') = y_{WH-3} = y_{WH\ \alpha} = \frac{\sum_{k=1}^{k_{max}} \alpha_k y_{\alpha_k}}{\sum_{k=1}^{k_{max}} \alpha_k} \tag{1}$$

This proposal uses the average of the contribution of each level which includes the horizontal level-α_0 or IT2α_0 FLS output, y_{α_0}, giving $N+1$ levels:

$$f_{EWH\ IT3\ NSFLS-1}(\boldsymbol{x}') = y_{EWH-3} = y_{EWH\ \alpha} = y_\alpha = \frac{\sum_{k=0}^{N} y_{\alpha_k}}{N+1} \tag{2}$$

Remark 1. *Equation (2) presents one of the novelties of this paper that represents the enhancement of the Wagner-Hagras model adding the level-α_0 that provide the basis for the evaluation of overall IT3 system and determines their performance as in the case of the predecessor IT2 model.*

$$y_{\alpha_k} = \left[\frac{y_{l\alpha_k} + y_{r\alpha_k}}{2}\right] \tag{3}$$

$$f_{EWH\ IT3\ NSFLS-1}(\boldsymbol{x}') = y_\alpha = \frac{\sum_{k=0}^{N}\left[\left(y_{l,\alpha_k}^{cos}(x') + y_{r,\alpha_k}^{cos}(x')\right)/2\right]}{N+1} \tag{4}$$

where y_{l,α_k}^{cos} and y_{r,α_k}^{cos} are the left and right points of the center of sets of each y_{α_k}, and its union can be expressed as an expansion y_{EWH-3} composed by $N+1$ elements y_{α_k} corresponding to the $N+1$ horizontal levels-α_k:

$$y_\alpha = \frac{1}{N+1} y_{\alpha_0} + \frac{1}{N+1} y_{\alpha_1} + \frac{1}{N+1} y_{\alpha_2} + \cdots + \frac{1}{N+1} y_{\alpha_k} + \cdots + \frac{1}{N+1} y_{\alpha_N} \tag{5}$$

Each weighted output y_{α_k} corresponding to each level-α_k can be calculated using the EWH IT3 NFLS-1 modeling with the uncertain level-$\alpha_k \in [\underline{\alpha}_k, \overline{\alpha}_k]$. Now the proposed y_{EWH-3} expansion is composed by $2N+2$ elements, (11).

$$y_\alpha = \frac{1}{N+1}\left(\frac{\underline{\alpha}_0 y_{\underline{\alpha}_0} + \overline{\alpha}_0 y_{\overline{\alpha}_0}}{\underline{\alpha}_0 + \overline{\alpha}_0}\right) + \frac{1}{N+1}\left(\frac{\underline{\alpha}_1 y_{\underline{\alpha}_1} + \overline{\alpha}_1 y_{\overline{\alpha}_1}}{\underline{\alpha}_1 + \overline{\alpha}_1}\right) + \cdots + \frac{1}{N+1}\left(\frac{\underline{\alpha}_k y_{\underline{\alpha}_k} + \overline{\alpha}_k y_{\overline{\alpha}_k}}{\underline{\alpha}_k + \overline{\alpha}_k}\right) + \cdots + \frac{1}{N+1}\left(\frac{\underline{\alpha}_N y_{\underline{\alpha}_N} + \overline{\alpha}_N y_{\overline{\alpha}_N}}{\underline{\alpha}_N + \overline{\alpha}_N}\right) \tag{6}$$

$$y_\alpha = \frac{1}{N+1}\left(\frac{\underline{\alpha}_0}{\underline{\alpha}_0 + \overline{\alpha}_0}\right) y_{\underline{\alpha}_0} + \frac{1}{N+1}\left(\frac{\overline{\alpha}_0}{\underline{\alpha}_0 + \overline{\alpha}_0}\right) y_{\overline{\alpha}_0} + \frac{1}{N+1}\left(\frac{\underline{\alpha}_1}{\underline{\alpha}_1 + \overline{\alpha}_1}\right) y_{\underline{\alpha}_1} + \frac{1}{N+1}\left(\frac{\overline{\alpha}_1}{\underline{\alpha}_1 + \overline{\alpha}_1}\right) y_{\overline{\alpha}_1} + \cdots + \frac{1}{N+1}\left(\frac{\underline{\alpha}_k}{\underline{\alpha}_k + \overline{\alpha}_k}\right) y_{\underline{\alpha}_k} + \frac{1}{N+1}\left(\frac{\overline{\alpha}_k}{\underline{\alpha}_k + \overline{\alpha}_k}\right) y_{\overline{\alpha}_k} + \cdots + \frac{1}{N+1}\left(\frac{\underline{\alpha}_N}{\underline{\alpha}_N + \overline{\alpha}_N}\right) y_{\underline{\alpha}_N} + \frac{1}{N+1}\left(\frac{\overline{\alpha}_N}{\underline{\alpha}_N + \overline{\alpha}_N}\right) y_{\overline{\alpha}_N} \tag{7}$$

$$y_\alpha = K_{\underline{\alpha}_0} y_{\underline{\alpha}_0} + K_{\overline{\alpha}_0} y_{\overline{\alpha}_0} + K_{\underline{\alpha}_1} y_{\underline{\alpha}_1} + K_{\overline{\alpha}_1} y_{\overline{\alpha}_1} + \cdots + K_{\underline{\alpha}_k} y_{\underline{\alpha}_k} + K_{\overline{\alpha}_k} y_{\overline{\alpha}_k} + \cdots + K_{\underline{\alpha}_N} y_{\underline{\alpha}_N} + K_{\overline{\alpha}_N} y_{\overline{\alpha}_N} \tag{8}$$

Now y_α the output of the EWH IT3 NSFLS-1 can be modeled as EWH GT2 NSFLS-1 system composed by $2N+2$ elements.

where

$$K_{\alpha_0} = \frac{1}{N+1}\left[\frac{\underline{\alpha}_0}{\underline{\alpha}_0 + \overline{\alpha}_0}\right]$$

Preprints (www.preprints.org) | NOT PEER-REVIEWED | Posted: 31 October 2023 doi:10.20944/preprints202310.2072.v1

$$K_{\alpha_1} = \frac{1}{N+1}\left[\frac{\overline{\alpha}_0}{\underline{\alpha}_0+\overline{\alpha}_0}\right]$$

$$K_{\alpha_2} = \frac{1}{N+1}\left[\frac{\underline{\alpha}_1}{\underline{\alpha}_1+\overline{\alpha}_1}\right]$$

$$K_{\alpha_3} = \frac{1}{N+1}\left[\frac{\overline{\alpha}_1}{\underline{\alpha}_1+\overline{\alpha}_1}\right]$$

$$\vdots$$

$$K_{\alpha_k} = \frac{1}{N+1}\left[\frac{\underline{\alpha}_k}{\underline{\alpha}_k+\overline{\alpha}_k}\right]$$

$$K_{\alpha_{k+1}} = \frac{1}{N+1}\left[\frac{\overline{\alpha}_k}{\underline{\alpha}_k+\overline{\alpha}_k}\right]$$

$$\vdots$$

$$K_{\alpha_{2N+1}} = \frac{1}{N+1}\left[\frac{\underline{\alpha}_{N+1}}{\underline{\alpha}_{N+1}+\overline{\alpha}_{N+1}}\right]$$

$$K_{\alpha_{2N+2}} = \frac{1}{N+1}\left[\frac{\overline{\alpha}_{N+1}}{\underline{\alpha}_{N+1}+\overline{\alpha}_{N+1}}\right] \quad (9)$$

and:

$$y_{\alpha_0} = y_{\underline{\alpha}_0}$$

$$y_{\alpha_1} = y_{\overline{\alpha}_0}$$

$$\vdots$$

$$y_{\alpha_k} = y_{\underline{\alpha}_k}$$

$$y_{\alpha_{k+1}} = y_{\overline{\alpha}_{k+1}}$$

$$\vdots$$

$$y_{\alpha_{2N+1}} = y_{\underline{\alpha}_{N+1}}$$

$$y_{\alpha_{2N+2}} = y_{\overline{\alpha}_{N+1}} \quad (10)$$

then:

$$y_\alpha = K_{\alpha_0}\left[\frac{y_{l\underline{\alpha}_0}+y_{r\underline{\alpha}_0}}{2}\right] + K_{\alpha_1}\left[\frac{y_{l\overline{\alpha}_0}+y_{r\overline{\alpha}_0}}{2}\right] + \ldots +$$

$$K_{\alpha_k}\left[\frac{y_{l\underline{\alpha}_k}+y_{r\underline{\alpha}_k}}{2}\right] + K_{\alpha_{k+1}}\left[\frac{y_{l\overline{\alpha}_{k+1}}+y_{r\overline{\alpha}_{k+1}}}{2}\right] + \cdots +$$

$$K_{\alpha_{2N+1}}\left[\frac{y_{l\underline{\alpha}_N}+y_{r\underline{\alpha}_N}}{2}\right] + K_{\alpha_{2N+2}}\left[\frac{y_{l\overline{\alpha}_N}+y_{r\overline{\alpha}_N}}{2}\right] \quad (11)$$

$$y_\alpha = \sum_{k=0}^{2N+2} K_{\alpha_k} y_{\alpha_k} \quad (12)$$

The centroids can be calculated with the centroid equations using the Karnik-Mendel (KM) algorithm for any left endpoint $y_{l\alpha_k}$:

$$y_{l\alpha_k} = \frac{\sum_{n=1}^{L} \overline{f}_{\alpha_k}^{n} * c_{l\alpha_k}^{n} + \sum_{n=L+1}^{M} \underline{f}_{\alpha_k}^{n} * c_{l\alpha_k}^{n}}{\sum_{n=1}^{L} \overline{f}_{\alpha_k}^{n} + \sum_{n=L+1}^{M} \underline{f}_{\alpha_k}^{n}} \quad (13)$$

for any right endpoint $y_{r\alpha_k}$:

Preprints (www.preprints.org) | NOT PEER-REVIEWED | Posted: 31 October 2023 doi:10.20944/preprints202310.2072.v1

$$y_{r\alpha_k} = \frac{\sum_{n=1}^{R} \underline{f}_{\alpha_k}^{n} * c_{r\alpha_k}^{n} + \sum_{n=R+1}^{M} \overline{f}_{\alpha_k}^{n} * c_{r\alpha_k}^{n}}{\sum_{n=1}^{R} \underline{f}_{\alpha_k}^{n} + \sum_{n=R+1}^{M} \overline{f}_{\alpha_k}^{n}} \quad (14)$$

$\left[\underline{f}_{\alpha_k}^{n}, \overline{f}_{\alpha_k}^{n}\right]$ is the estimated firing interval and $\left[c_{l\alpha_k}^{n}, c_{r\alpha_k}^{n}\right]$ is the estimated consequent centroid of the rule n of the level-α_k.

2.1.1. Input Variables, Rules, and Levels-α_k

The designer must select $q = 1, 2, \ldots, p$ the input variables, $i = 1, 2, \ldots, M$ the number of rules, $k = 1, 2, \ldots, N$, the initial number of horizontal levels-α_k to start the construction of the EWH IT3 NSFLS-1 system with the design and construction of the IT2α_0 FLS.

The p inputs are type-1 non-singleton numbers modeled as a Gaussian with the mean x_q' and a standard deviation σ_{X_q}. The well-known type-1 non-singleton Gaussian model is used as primary MF:

$$\mu_{\tilde{X}_q}(x_q) = exp\left[-\frac{1}{2}\left[\frac{x_q - x_q'}{\sigma_{X_q}}\right]^2\right] \quad (15)$$

Each input must cover its universe of discourse (UOD) with the required number of MFs.

2.1.2. The Membership Functions and Universe of Discourse

The number M of rules is determined by the array of required MFs of each input. If there are two inputs, and the UOD of $\tilde{X}_1$ and $\tilde{X}_2$ are covered by five MFs each, then the rule base has M = 5x5 = 25 rules.

Each consequent MF is modeled as Gaussian with uncertain means $M_q^i \in \left[M_{q_1}^i, M_{q_2}^i\right]$ and common standard deviation σ_q^i:

$$\mu_{\tilde{A}_q^i}(x_q) = exp\left[-\frac{1}{2}\left[\frac{x_q - M_q^i}{\sigma_q^i}\right]^2\right] \quad (16)$$

The IT3 Mamdani fuzzy rule base model has p inputs $x_1 \in X_1, \ldots, x_p \in X_p$, one output $\in Y$, and a rule base of size M of the form:

$$\tilde{R}^i: IF\ x_1\ is\ \tilde{A}_1^i\ and \ldots and\ x_p\ is\ \tilde{A}_p^i\ THEN\ y\ is\ \tilde{G}^i \quad (17)$$

where $q = 1, 2, \ldots, p$ is the number of inputs; $i = 1, 2, \ldots, M$ is the number of rules.

2.1.3. The Rule Base

The rule base of the horizontal level-α_0, is constructed assigning the initial values of each of the pM membership functions, $\tilde{A}_1^i, \tilde{A}_2^i \ldots \tilde{A}_p^i$, and M consequent centroids $\left[\underline{c}_{l\alpha_0}^i, \overline{c}_{r\alpha_0}^i\right]$.

$$\tilde{R}^i: IF\ x_1\ is\ \tilde{A}_1^i\ and \ldots\ x_p\ is\ \tilde{A}_p^i\ THEN\ y\ is\ \left[\underline{c}_{l\alpha_0}^i, \overline{c}_{r\alpha_0}^i\right] \quad (18)$$

2.1.4. Alpha α_k-Cuts

The M firing intervals $\left[\underline{f}_{l\alpha_0}^i, \overline{f}_{r\alpha_0}^i\right]$ of the horizontal level-α_0 or IT2α_0 FLS are calculated based on (19) using the α_0-cuts or the intersection of x_q' and the MF of each input and each rule. Only the α_0-cuts of level-α_0 are calculated, not the α_k-cuts of any other level-α_k.

$$\left[\underline{f}_{l\alpha_0}^i, \overline{f}_{r\alpha_0}^i\right] = \left[\prod_{q=1}^{p} a_{q\alpha_0}^i\left(\underline{x}_{q,max}^i\right), \prod_{q=1}^{p} b_{q\alpha_0}^i\left(\overline{x}_{q,max}^i\right)\right] \quad (19)$$

Preprints (www.preprints.org) | NOT PEER-REVIEWED | Posted: 31 October 2023 doi:10.20944/preprints202310.2072.v1

with

$$a^i_{q\alpha_0}\left(\underline{x}^i_{q,max}\right) = \underline{\mu}_{\tilde{x}_q}(\underline{x}^i_{q,max})\underline{\mu}_{\tilde{A}^i_q}(\underline{x}^i_{q,max}) \tag{20}$$

and

$$b^i_{q\alpha_0}\left(\overline{x}^i_{q,max}\right) = \overline{\mu}_{\tilde{x}_q}(\overline{x}^i_{q,max})\overline{\mu}_{\tilde{A}^i_q}(\overline{x}^i_{q,max}) \tag{21}$$

$\underline{x}^i_{q,max}$ and $\overline{x}^i_{q,max}$ are determined according to the locations of x'_q with respect to M^i_{q1} and M^i_{q2} as it is shown in Table 4.

Table 4. Locations of x'_q, for $\underline{x}^i_{q,max}$ and $\overline{x}^i_{q,max}$ estimation used to calculate $\left[\underline{f}^i_{l\alpha_0}, \overline{f}^i_{r\alpha_0}\right]$ and $\left[\underline{f}^i_{l\alpha_k}, \overline{f}^i_{r\alpha_k}\right]$.

	Location of x'_q for $\underline{x}^i_{q,max}$ calculation	Location of x'_q for $\overline{x}^i_{q,max}$ Calculation	$\underline{x}^i_{q,max}$	$\overline{x}^i_{q,max}$
1	$x'_q < \frac{M^i_{q1\alpha_0} + M^i_{q2\alpha_0}}{2} - \frac{\left(\sigma^i_{x_{q1}}\right)^2 \left(M^i_{q2\alpha_0} - M^i_{q1\alpha_0}\right)}{2\left(\sigma^i_{q\alpha_0}\right)^2}$	$x'_q < M^i_{q1\alpha_0}$	$\underline{x}^i_{q,max} = \frac{\left(\sigma^i_{x_{q1}}\right)^2 M^i_{q2\alpha_0} + \left(\sigma^i_q\right)^2 x'_q}{\left(\sigma^i_{x_{q1}}\right)^2 + \left(\sigma^i_{q\alpha_0}\right)^2}$	$\overline{x}^i_{q,max} = \frac{\left(\sigma^i_{x_{q2}}\right)^2 M^i_{q1\alpha_0} + \left(\sigma^i_q\right)^2 x'_q}{\left(\sigma^i_{x_{q2}}\right)^2 + \left(\sigma^i_{q\alpha_0}\right)^2}$
2	$x'_q < \frac{M^i_{q1\alpha_0} + M^i_{q2\alpha_0}}{2} - \frac{\left(\sigma^i_{x_{q1}}\right)^2 \left(M^i_{q2\alpha_0} - M^i_{q1\alpha_0}\right)}{2\left(\sigma^i_{q\alpha_0}\right)^2}$	$x'_q \in \left[M^i_{q1\alpha_0}, M^i_{q2\alpha_0}\right]$	$\underline{x}^i_{q,max} = \frac{\left(\sigma^i_{x_{q1}}\right)^2 M^i_{q2\alpha_0} + \left(\sigma^i_q\right)^2 x'_q}{\left(\sigma^i_{x_{q1}}\right)^2 + \left(\sigma^i_{q\alpha_0}\right)^2}$	$\overline{x}^i_{q,max} = x'_q$
3	$x'_q \in \left[\frac{M^i_{q1\alpha_0} + M^i_{q2\alpha_0}}{2} - \frac{\left(\sigma^i_{x_{q1}}\right)^2 \left(M^i_{q2\alpha_0} - M^i_{q1\alpha_0}\right)}{2\left(\sigma^i_{q\alpha_0}\right)^2}, \frac{M^i_{q1\alpha_0} + M^i_{q2\alpha_0}}{2} + \frac{\left(\sigma^i_{x_{q1}}\right)^2 \left(M^i_{q2\alpha_0} - M^i_{q1\alpha_0}\right)}{2\left(\sigma^i_{q\alpha_0}\right)^2}\right]$	$x'_q \in \left[M^i_{q1\alpha_0}, M^i_{q2\alpha_0}\right]$	$\underline{x}^i_{q,max} = \frac{M^i_{q1\alpha_0} + M^i_{q2\alpha_0}}{2}$	$\overline{x}^i_{q,max} = x'_q$
4	$x'_q > \frac{M^i_{q1\alpha_0} + M^i_{q2\alpha_0}}{2} + \frac{\left(\sigma^i_{x_{q1}}\right)^2 \left(M^i_{q2\alpha_0} - M^i_{q1\alpha_0}\right)}{2\left(\sigma^i_{q\alpha_0}\right)^2}$	$x'_q \in \left[M^i_{q1\alpha_0}, M^i_{q2\alpha_0}\right]$	$\underline{x}^i_{q,max} = \frac{\left(\sigma^i_{x_{q1}}\right)^2 M^i_{q1\alpha_0} + \left(\sigma^i_q\right)^2 x'_q}{\left(\sigma^i_{x_{q1}}\right)^2 + \left(\sigma^i_{q\alpha_0}\right)^2}$	$\overline{x}^i_{q,max} = x'_q$
5	$x'_q > \frac{M^i_{q1\alpha_0} + M^i_{q2\alpha_0}}{2} + \frac{\left(\sigma^i_{x_{q1}}\right)^2 \left(M^i_{q2\alpha_0} - M^i_{q1\alpha_0}\right)}{2\left(\sigma^i_{q\alpha_0}\right)^2}$	$x'_q > M^i_{q2}$	$\underline{x}^i_{q,max} = \frac{\left(\sigma^i_{x_{q1}}\right)^2 M^i_{q1\alpha_0} + \left(\sigma^i_q\right)^2 x'_q}{\left(\sigma^i_{x_{q1}}\right)^2 + \left(\sigma^i_{q\alpha_0}\right)^2}$	$\overline{x}^i_{q,max} = \frac{\left(\sigma^i_{x_{q2}}\right)^2 M^i_{q2\alpha_0} + \left(\sigma^i_q\right)^2 x'_q}{\left(\sigma^i_{x_{q2}}\right)^2 + \left(\sigma^i_{q\alpha_0}\right)^2}$

Preprints (www.preprints.org) | NOT PEER-REVIEWED | Posted: 31 October 2023 doi:10.20944/preprints202310.2072.v1

2.1.5. Firing Intervals

Each firing interval $\left[\underline{f}^i_{l\alpha_0}, \overline{f}^i_{r\alpha_0}\right]$ of the horizontal level-α_0 or IT2α_0 NSFLS-1 is used to estimate the antecedent's firing interval of each level-$\alpha_k \in [\underline{\alpha}_k, \overline{\alpha}_k]$. As it is shown in Figure 5, the Gaussian model of the vertical slice at $x'_{q,max}$ used to calculate the firing interval $\left[\underline{f}^i_{l\alpha_k}, \overline{f}^i_{r\alpha_k}\right]$ of each level-α_k is:

$$\mu_{f^i_{vs\alpha_k}} = \alpha_k = exp\left[-\frac{1}{2}\left[\frac{x'_q - m^i_{fvs\alpha_0}}{\sigma^i_{fvs\alpha_0}}\right]^2\right] \tag{22}$$

where

$$m^i_{f_{vs\alpha_0}} = \frac{\underline{f}^i_{l\alpha_0} + \overline{f}^i_{r\alpha_0}}{2} \tag{23}$$

$$\sigma^i_{f_{vs\alpha_0}} = \frac{\overline{f}^i_{r\alpha_0} - \underline{f}^i_{l\alpha_0}}{z} \tag{24}$$

$$\left[\underline{f}^i_{l\alpha_k}, \overline{f}^i_{r\alpha_k}\right] = \frac{\underline{f}^i_{l\alpha_0} + \overline{f}^i_{r\alpha_0}}{2} \mp \frac{\overline{f}^i_{r\alpha_0} - \underline{f}^i_{l\alpha_0}}{z} \sqrt[2]{-2\ln(\alpha_k)} \tag{25}$$

with z = 1, 2, …,n being an integer number estimated by trial and error. The magnitude of the standard deviation of the model is a fraction of the interval of the means.

a)

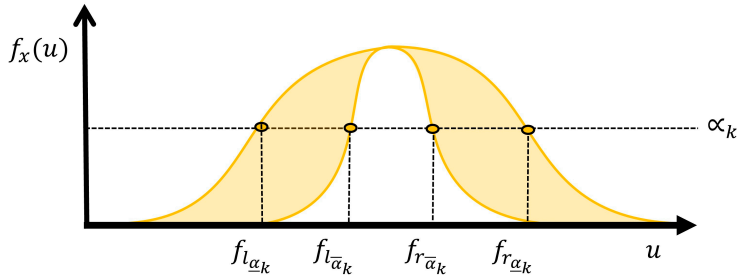

b)

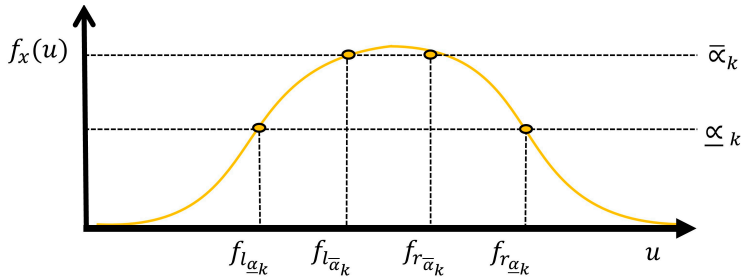

Figure 5. Geometrical view used to calculate, a) For each level-$\boldsymbol{\alpha_k}$, each $\boldsymbol{\alpha_k}$-cut point of the firing interval of the antecedent section of the proposed EWH IT3 NSFLS-1 systems, and b) Its equivalent geometrical view in GT2 systems.

2.1.6. Consequent Centroids

Each consequent's centroids $\left[\underline{c}^i_{l\alpha_0}, \overline{c}^i_{r\alpha_0}\right]$ of the horizontal level-α_0 are used to estimate the M consequents' centroid of the level-$\alpha_k \in [\underline{\alpha}_k, \overline{\alpha}_k]$. As shown in Figure 6, the Gaussian model of the vertical slice at $x'_{q,max}$ used to calculate the centroid $\left[\underline{c}^i_{l\alpha_k}, \overline{c}^i_{r\alpha_k}\right]$ of each level-α_k is:

$$\mu_{c^i_{vs\alpha_k}} = \alpha_k = exp\left[-\frac{1}{2}\left[\frac{x'_q - m^i_{cvs\alpha_0}}{\sigma^i_{cvs\alpha_0}}\right]^2\right] \tag{26}$$

where

Preprints (www.preprints.org) | NOT PEER-REVIEWED | Posted: 31 October 2023 doi:10.20944/preprints202310.2072.v1

$$m^i_{cvs\alpha_0} = \frac{c^i_{l\alpha_0} + \overline{c}^i_{r\alpha_0}}{2} \tag{27}$$

$$\sigma^i_{cvs\alpha_0} = \frac{\overline{c}^i_{r\alpha_0} - c^i_{l\alpha_0}}{z} \tag{28}$$

$$\left[\underline{c}^i_{l\alpha_k}, \overline{c}^i_{r\alpha_k}\right] = \frac{c^i_{l\alpha_0} + \overline{c}^i_{r\alpha_0}}{2} \mp \frac{\overline{c}^i_{r\alpha_0} - c^i_{l\alpha_0}}{z} \sqrt[2]{-2\ln(\alpha_k)} \tag{29}$$

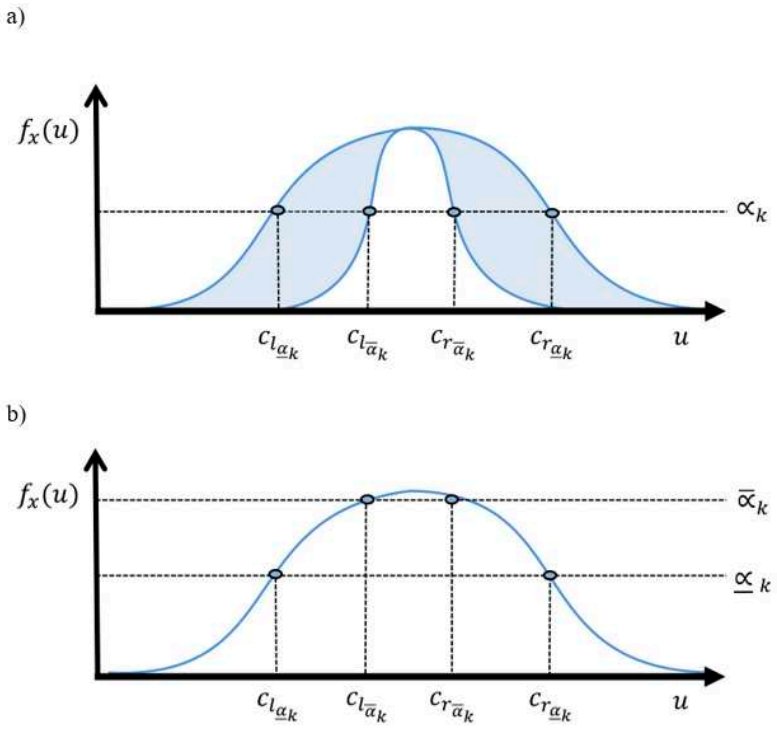

Figure 6. Geometrical view used to calculate, a) For each level-$\boldsymbol{\alpha_k}$, each $\boldsymbol{\alpha_k}$-cut point of the Centroids of the consequent section of the proposed EWH IT3 NSFLS-1 system, and b) its equivalent geometrical view in GT2 systems.

2.1.7. Expansion of the Level-α_k

The proposed EWH IT3 NSFLS-1 solves the processing of the uncertainty of the secondary grade of each level-α_k, Figure 1, by replacing this level by its two levels-α_k that represent the uncertainty in the secondary membership: The lower level-$\underline{\alpha}_k$ and the upper level-$\overline{\alpha}_k$. Now the expanded number of the horizontal levels-α_k is $2N+2$, transforming the EWH IT3 NSFLS-1 into a EWH GT2 NSFLS-1 system, by applying the EWH GT2 methodology to $2N+2$ levels-α_k (8).

2.1.8. Calculation of y_α

For each input-output training data pair $(\boldsymbol{x}', y)$, y_α can be estimated using (12). The proposed EWH IT3 NSFLS-1 is dynamically constructed because its structure is calculated for each input vector $\boldsymbol{x}'_q$. The horizontal level-α_0 or IT2α_0 NSFLS-1 is used as the base line to estimate the structure of each horizontal level-α_k or IT2α_k. Regardless of it being either the low horizontal level-$\underline{\alpha}_k$ or the upper horizontal level-$\overline{\alpha}_k$, it requires the same procedure: In each level-α_k an IT2α_k NSFLS-1 is constructed with its corresponding antecedent firing interval $\left[\underline{f}^i_{l\alpha_k}, \overline{f}^i_{r\alpha_k}\right]$ and its corresponding consequent centroid $\left[\underline{c}^i_{l\alpha_k}, \overline{c}^i_{r\alpha_k}\right]$. An important characteristic is that the estimated parameters of the antecedent and consequent sections of each rule of all the levels-$\alpha_k \in \left[\underline{\alpha}_k, \overline{\alpha}_k\right]$ are dynamic and temporal, and

Preprints (www.preprints.org) | NOT PEER-REVIEWED | Posted: 31 October 2023 doi:10.20944/preprints202310.2072.v1

only the parameters of the level-α_0 or IT2α_0 are permanent. Only the level-α_0 has MF parameters of its Gaussians models, while any other level-α_k temporarily has the corresponding estimated firing intervals $\left[\underline{f}^i_{l\alpha_k}, \overline{f}^i_{r\alpha_k}\right]$ and the estimated centroids $\left[\underline{c}^i_{l\alpha_k}, \overline{c}^i_{r\alpha_k}\right]$ both required to calculate its contribution to the final value y_α. To estimate the value y_α we propose the average using each output y_{α_k}: $y_\alpha = \frac{\sum_{k=1}^{kmax} y_{\alpha_k}}{N}$.

2.2. The BP Method for Antecedent Tunning

An objective function $E(\theta)$ may have a non-linear form with respect to an adjustable parameter θ. In the interactive descent methods, the next point $\theta(new)$ is determined by one step down from the current point $\theta(now)$ in the negative direction of the gradient of the function $E(\theta_{now})$. The K learning rates are selected by trial and error while meeting the selected criteria of minimizing the error.

$$\theta(new) = \theta(now) - Kg \tag{30}$$

$$\theta(new) = \theta(now) - K\,\frac{\partial E}{\partial \theta_{now}} \tag{31}$$

K is the training rate, and g is the vector of the first partial derivatives of $E(\theta)$ and is equivalent to $\frac{\partial E}{\partial \theta_{now}}$:

$$g(\theta) = \left[\frac{\partial E}{\partial \theta_{1\,now}}, \frac{\partial E}{\partial \theta_{2\,now}}, \ldots, \frac{\partial E}{\partial \theta_{n\,now}}\right]^T \tag{32}$$

Each rule of the level-α_0 applies equation (32) to update three θ antecedent parameters, $M^i_{q1\alpha_0}$, $M^i_{q2\alpha_0}$, and $\sigma^i_{q\alpha_0}$.

Equation (32) requires finding the partial derivatives used to update all the parameters of the antecedent section of each rule of only the IT2α_0 NFLS-2 located at level-α_0.

$$M^i_{q1\alpha_0}(new) = M^i_{q1\alpha_0}(now) - K_{M_{q1\alpha_0}}\frac{\partial E}{\partial M^i_{q1\alpha_0}} \tag{33}$$

$$M^i_{q2\alpha_0}(new) = M^i_{q2\alpha_0}(now) - K_{M_{q2\alpha_0}}\frac{\partial E}{\partial M^i_{q2\alpha_0}} \tag{34}$$

$$\sigma^i_{q\alpha_0}\ (new)\ = \sigma^i_{q\alpha_0}(now) - K_{\sigma_q\alpha_0}\frac{\partial E}{\partial \sigma^i_{q\alpha_0}} \tag{35}$$

where $K_{M_{q1\alpha_0}}$, $K_{M_{q2\alpha_0}}$, and $K_{\sigma_q\alpha_0}$, are the training rates of its corresponding parameter.

The quadratic error function to minimize is:

$$E = \frac{1}{2}(y - y_\alpha)^2 \tag{36}$$

where: y is the output value of the L input-output data pairs. The error function is:

$$e = y - y_\alpha \tag{37}$$

As an example, the logic sequence of the math steps to obtain the partial derivatives of the objective function E with respect to the antecedent parameter $M^i_{q1\alpha_0}$ are illustrated from (38) to (40).

$$M^i_{q1\alpha_0}(new) = M^i_{q1\alpha_0}(now) - K_{M_{q1\alpha_0}}\frac{\partial E}{\partial M^i_{q1\alpha_0}} \tag{38}$$

then

$$\frac{\partial E}{\partial M^i_{q1\alpha_0}} = \left[\frac{\partial E}{\partial y_\alpha}\frac{\partial y_\alpha}{\partial y_{\underline{\alpha}_1}}\frac{\partial y_{\underline{\alpha}_1}}{\partial M^i_{q1\alpha_0}} + \frac{\partial E}{\partial y_\alpha}\frac{\partial y_\alpha}{\partial y_{\overline{\alpha}_1}}\frac{\partial y_{\overline{\alpha}_1}}{\partial M^i_{q1\alpha_0}} + \cdots + \frac{\partial E}{\partial y_\alpha}\frac{\partial y_\alpha}{\partial y_{\underline{\alpha}_k}}\frac{\partial y_{\underline{\alpha}_k}}{\partial M^i_{q1\alpha_0}} + \frac{\partial E}{\partial y_\alpha}\frac{\partial y_\alpha}{\partial y_{\overline{\alpha}_k}}\frac{\partial y_{\overline{\alpha}_k}}{\partial M^i_{q1\alpha_0}} + \cdots + \frac{\partial E}{\partial y_\alpha}\frac{\partial y_\alpha}{\partial y_{\underline{\alpha}_N}}\frac{\partial y_{\underline{\alpha}_N}}{\partial M^i_{q1\alpha_0}} + \frac{\partial E}{\partial y_\alpha}\frac{\partial y_\alpha}{\partial y_{\overline{\alpha}_N}}\frac{\partial y_{\overline{\alpha}_N}}{\partial M^i_{q1\alpha_0}}\right] \tag{39}$$

Preprints (www.preprints.org) | NOT PEER-REVIEWED | Posted: 31 October 2023 doi:10.20944/preprints202310.2072.v1

which is equivalent to:

$$\frac{\partial E}{\partial M^i_{q1\alpha_0}} = \left[\frac{\partial E}{\partial y_\alpha}\frac{\partial y_\alpha}{\partial y_{\alpha_1}}\frac{\partial y_{\alpha_1}}{\partial M^i_{q1\alpha_0}} + \frac{\partial E}{\partial y_\alpha}\frac{\partial y_\alpha}{\partial y_{\alpha_2}}\frac{\partial y_{\alpha_2}}{\partial M^i_{q1\alpha_0}} + \cdots + \frac{\partial E}{\partial y_\alpha}\frac{\partial y_\alpha}{\partial y_{\alpha_k}}\frac{\partial y_{\alpha_k}}{\partial M^i_{q1\alpha_0}} + \cdots + \frac{\partial E}{\partial y_\alpha}\frac{\partial y_\alpha}{\partial y_{\alpha_N}}\frac{\partial y_{\alpha_N}}{\partial M^i_{q1\alpha_0}} + \cdots \frac{\partial E}{\partial y_\alpha}\frac{\partial y_\alpha}{\partial y_{\alpha_{2N}}}\frac{\partial y_{\alpha_{2N}}}{\partial M^i_{q1\alpha_0}}\right] \quad (40)$$

Each level-$\alpha_k \in [\underline{\alpha}_k, \overline{\alpha}_k]$ previously defined during the construction process, contributes only by updating the parameters of the permanent level-α_0. No parameters of the level-α_k have training only have it the level-α_0 parameters.

A similar procedure can be used to calculate the equations for training: $M^i_{q2\alpha_0}$, and $\sigma^i_{q\alpha_0}$ of the IT2α_0 NSFLS-1.

As shown in Table 4, the final equations for training the parameters of the antecedent depend on the relative position of x'_q with respect to $M^i_{q1\alpha_0}$ and $M^i_{q2\alpha_0}$ positions. Table 5 shows the complete set of equations for parameters $M^i_{q1\alpha_0}$, $M^i_{q2\alpha_0}$ and $\sigma^i_{q\alpha_0}$, with training under y_l contribution. Table 6 also shows the complete set of equations for training these three antecedent parameters under the y_r contribution.

Table 5. Gradient descent equations for antecedent training under y_l contribution.

	Location of x'_q		**Parameter of the antecedent membership function that contributes to the left-most section**
1	$x'_q \le M^i_{q1\alpha_0}$	$\overline{f}^i_{r\alpha_k} \in \left(\overline{f}^1_{r\alpha_k} \ldots \overline{f}^L_{r\alpha_k}\right)$	$M^i_{q1\alpha_0}(new) = M^i_{q1\alpha_0}(now) + \frac{1}{2}K_{M_{q1\alpha_0}} e \sum_{k=0}^{2N+2} K_{\alpha_k}\left[\frac{\underline{c}^i_{l\alpha_k} - y_{l\alpha_k}}{\sum_{j=1}^{L}\overline{f}^j_{r\alpha_k} + \sum_{j=L+1}^{M}\underline{f}^j_{l\alpha_k}}\right]\left[\frac{1}{2} + \frac{\sqrt[2]{-2\ln(\alpha_k)}}{z}\right]\left[\left(\frac{x'_q - M^i_{q1\alpha_0}}{\left(\sigma^i_{q\alpha_0}\right)^2 + \left(\sigma^i_{x_{q2}}\right)^2}\right)\overline{f}^i_{r\alpha_0}\right]$
			$\sigma^i_{q\alpha_0}(new) = \sigma^i_{q\alpha_0}(now) + \frac{1}{2}K_{\sigma_{q\alpha_0}} e \sum_{k=0}^{2N+2} K_{\alpha_k}\left[\frac{\underline{c}^i_{l\alpha_k} - y_{l\alpha_k}}{\sum_{j=1}^{L}\overline{f}^j_{r\alpha_k} + \sum_{j=L+1}^{M}\underline{f}^j_{l\alpha_k}}\right]\left[\frac{1}{2} + \frac{\sqrt[2]{-2\ln(\alpha_k)}}{z}\right]\left[\sigma^i_{q\alpha_0}\right]\left[\frac{\left(x'_q - M^i_{q1\alpha_0}\right)^2}{\left[\left(\sigma^i_{q\alpha_0}\right)^2 + \left(\sigma^i_{x_{q2}}\right)^2\right]^2}\overline{f}^i_{r\alpha_0}\right]$
2	$x'_q \ge M^i_{q2\alpha_0}$	$\overline{f}^i_{r\alpha_k} \in \left(\overline{f}^1_{r\alpha_k} \ldots \overline{f}^L_{r\alpha_k}\right)$	$M^i_{q2\alpha_0}(new) = M^i_{q2\alpha_0}(now) + \frac{1}{2}K_{M_{q2\alpha_0}} e \sum_{k=0}^{2N+2} K_{\alpha_k}\left[\frac{\underline{c}^i_{l\alpha_k} - y_{l\alpha_k}}{\sum_{j=1}^{L}\overline{f}^i_{r\alpha_k} + \sum_{j=L+1}^{M}\underline{f}^i_{l\alpha_k}}\right]\left(\frac{1}{2} + \frac{\sqrt[2]{-2\ln(\alpha_k)}}{z}\right)\left[\left(\frac{x'_q - M^i_{q2\alpha_0}}{\left(\sigma^i_{x_{q2}}\right)^2 + \left(\sigma^i_{q\alpha_0}\right)^2}\right)\overline{f}^i_{r\alpha_0}\right]$

Preprints (www.preprints.org) | NOT PEER-REVIEWED | Posted: 31 October 2023 doi:10.20944/preprints202310.2072.v1

			$\sigma^i_{q\alpha_0}(new)$ $= \sigma^i_{q\alpha_0}(now)$ $+\frac{1}{2}K_{\sigma_q\alpha_0}e\sum_{k=0}^{2N+2}K_{\alpha_k}\left[\frac{\underline{c}^i_{l\alpha_k}-y_{l\alpha_k}}{\sum_{j=1}^{L}\overline{f}^i_{r\alpha_k}+\sum_{j=L+1}^{M}\underline{f}^i_{l\alpha_k}}\right]\left[\frac{1}{2}\right.$ $\left.+\frac{\sqrt[2]{-2\,ln(\alpha_k)}}{z}\right]\left[\sigma^i_{q\alpha_0}\right]\left[\frac{\left(x'_q-M^i_{q2\alpha_0}\right)^2}{\left[\left(\sigma^i_{x_{q2}}\right)^2+\left(\sigma^i_{q\alpha_0}\right)^2\right]^2}\overline{f}^i_{r\alpha_0}\right]$
3	x'_q $\leq \frac{M^i_{q1\alpha_0}+M^i_{q2\alpha_0}}{2}$ $-\frac{\left(\sigma^i_{x_{q1}}\right)^2\left(M^i_{q2\alpha_0}-M^i_{q1\alpha_0}\right)}{2\left(\sigma^i_{q\alpha_0}\right)^2}$	$\underline{f}^i_{l\alpha_k}$ $\in\left(\underline{f}^{L+1}_{l\alpha_k}\ldots\underline{f}^{M}_{l\alpha_k}\right)$	$M^i_{q2\alpha_0}(new)$ $= M^i_{q2\alpha_0}(now)$ $+\frac{1}{2}K_{M_{q2\alpha_0}}e\sum_{k=0}^{2N+2}K_{\alpha_k}\left[\frac{\underline{c}^i_{l\alpha_k}-y_{l\alpha_k}}{\sum_{j=1}^{L}\overline{f}^j_{r\alpha_k}+\sum_{j=L+1}^{M}\underline{f}^j_{l\alpha_k}}\right]\left(\frac{1}{2}\right.$ $\left.+\frac{\sqrt[2]{-2\,ln(\alpha_k)}}{z}\right)\left[\left(\frac{x'_q-M^i_{q2\alpha_0}}{\left(\sigma^i_{x_{q1}}\right)^2+\left(\sigma^i_{q\alpha_0}\right)^2}\right)\underline{f}^i_{l\alpha_0}\right]$
			$\sigma^i_{q\alpha_0}(new)$ $= \sigma^i_{q\alpha_0}(now)$ $+\frac{1}{2}K_{\sigma_q\alpha_0}e\sum_{k=0}^{2N+2}K_{\alpha_k}\left[\frac{\underline{c}^i_{l\alpha_k}-y_{l\alpha_k}}{\sum_{j=1}^{L}\overline{f}^j_{r\alpha_k}+\sum_{j=L+1}^{M}\underline{f}^j_{l\alpha_k}}\right]\left[\frac{1}{2}\right.$ $\left.+\frac{\sqrt[2]{-2\,ln(\alpha_k)}}{z}\right]\left[\sigma^i_{q\alpha_0}\right]\left[\frac{\left(x'_q-M^i_{q2\alpha_0}\right)^2}{\left[\left(\sigma^i_{x_{q1}}\right)^2+\left(\sigma^i_{q\alpha_0}\right)^2+\right]^2}\underline{f}^i_{l\alpha_0}\right]$
4	x'_q $\geq \frac{M^i_{q1\alpha_0}+M^i_{q2\alpha_0}}{2}$ $+\frac{\left(\sigma^i_{x_{q1}}\right)^2\left(M^i_{q2\alpha_0}-M^i_{q1\alpha_0}\right)}{2\left(\sigma^i_{q\alpha_0}\right)^2}$	$\underline{f}^i_{l\alpha_k}$ $\in\left(\underline{f}^{L+1}_{l\alpha_k}\ldots\underline{f}^{M}_{l\alpha_k}\right)$	$M^i_{q1\alpha_0}(new)$ $= M^i_{q1\alpha_0}(now)$ $+\frac{1}{2}K_{M_{q1\alpha_0}}e\sum_{k=0}^{2N+2}K_{\alpha_k}\left[\frac{\underline{c}^i_{l\alpha_k}-y_{l\alpha_k}}{\sum_{j=1}^{L}\overline{f}^j_{r\alpha_k}+\sum_{j=L+1}^{M}\underline{f}^j_{l\alpha_k}}\right]\left[\frac{1}{2}\right.$ $\left.+\frac{\sqrt[2]{-2\,ln(\alpha_k)}}{z}\right]\left[\left(\frac{x'_q-M^i_{q1}}{\left(\sigma^i_{x_{q1}}\right)^2+\left(\sigma^i_{q\alpha_0}\right)^2}\right)\underline{f}^i_{l\alpha_0}\right]$
			$\sigma^i_{q\alpha_0}(new)$ $= \sigma^i_{q\alpha_0}(now)$ $+\frac{1}{2}K_{\sigma_q\alpha_0}e\sum_{k=0}^{2N+2}K_{\alpha_k}\left[\frac{\underline{c}^i_{l\alpha_k}-y_{l\alpha_k}}{\sum_{j=1}^{L}\overline{f}^j_{r\alpha_k}+\sum_{j=L+1}^{M}\underline{f}^j_{l\alpha_k}}\right]\left[\frac{1}{2}\right.$ $\left.+\frac{\sqrt[2]{-2\,ln(\alpha_k)}}{z}\right]\left[\sigma^i_{q\alpha_0}\right]\left[\frac{\left(x'_q-M^i_{q1\alpha_0}\right)^2}{\left[\left(\sigma^i_{x_{q1}}\right)^2+\left(\sigma^i_{q\alpha_0}\right)^2\right]^2}\underline{f}^i_{l\alpha_0}\right]$

Table 6. Gradient descent equations for antecedent training under y_r contribution.

Preprints (www.preprints.org) | NOT PEER-REVIEWED | Posted: 31 October 2023 doi:10.20944/preprints202310.2072.v1

	Location of x'_q		Parameter of the antecedent membership function that contributes to the right-most section
1	$x'_q \le M^i_{q1\alpha_0}$	$\overline{f}^i_{r\alpha_k} \in \left(\overline{f}^{R+1}_{r\alpha_k} \dots \overline{f}^{M}_{r\alpha_k}\right)$	$M^i_{q1\alpha_0}(new) = M^i_{q1\alpha_0}(now) + \frac{1}{2}K_{M_{q1\alpha_0}} e \sum_{k=0}^{2N+2} K_{\alpha_k}\left[\frac{\overline{c}^i_{r\alpha_k} - y_{r\alpha_k}}{\sum_{j=1}^{R} \underline{f}^j_{l\alpha_k} + \sum_{j=R+1}^{M} \overline{f}^j_{r\alpha_k}}\right]\left[\frac{1}{2} + \frac{\sqrt[2]{-2\ln(\alpha_k)}}{z}\right]\left[\left(\frac{x'_q - M^i_{q1\alpha_0}}{\left(\sigma^i_{x_{q2}}\right)^2 + \left(\sigma^i_{q\alpha_0}\right)^2}\right)\overline{f}^i_{r\alpha_0}\right]$ $\sigma^i_{q\alpha_0}(new) = \sigma^i_{q\alpha_0}(now) + \frac{1}{2}K_{\sigma_{q\alpha_0}} e \sum_{k=0}^{2N+2} K_{\alpha_k}\left[\frac{\overline{c}^i_{r\alpha_k} - y_{r\alpha_k}}{\sum_{j=1}^{R} \underline{f}^i_{l\alpha_k} + \sum_{j=R+1}^{M} \overline{f}^j_{r\alpha_k}}\right]\left[\frac{1}{2} + \frac{\sqrt[2]{-2\ln(\alpha_k)}}{z}\right]\left[\sigma^i_{q\alpha_0}\right]\left[\frac{\left(x'_q - M^i_{q1\alpha_0}\right)^2}{\left[\left(\sigma^i_{x_{q2}}\right)^2 + \left(\sigma^i_{q\alpha_0}\right)^2\right]^2}\overline{f}^i_{r\alpha_0}\right]$
2	$x'_q \ge M^i_{q2\alpha_0}$	$\overline{f}^i_{r\alpha_k} \in \left(\overline{f}^{R+1}_{r\alpha_k} \dots \overline{f}^{M}_{r\alpha_k}\right)$	$M^i_{q2\alpha_0}(new) = M^i_{q2\alpha_0}(now) + \frac{1}{2}K_{M_{q2\alpha_0}} e \sum_{k=0}^{2N+2} K_{\alpha_k}\left[\frac{\overline{c}^i_{r\alpha_k} - y_{r\alpha_k}}{\sum_{j=1}^{R} \underline{f}^j_{l\alpha_k} + \sum_{j=R+1}^{M} \overline{f}^j_{r\alpha_k}}\right]\left(\frac{1}{2} + \frac{\sqrt[2]{-2\ln(\alpha_k)}}{z}\right)\left[\left(\frac{x'_q - M^i_{q2\alpha_0}}{\left(\sigma^i_{x_{q2}}\right)^2 + \left(\sigma^i_{q\alpha_0}\right)^2}\right)\overline{f}^i_{r\alpha_0}\right]$ $\sigma^i_{q\alpha_0}(new) = \sigma^i_{q\alpha_0}(now) + \frac{1}{2}K_{\sigma_{q\alpha_0}} e \sum_{k=0}^{2N+2} K_{\alpha_k}\left[\frac{\overline{c}^i_{r\alpha_k} - y_{r\alpha_k}}{\sum_{j=1}^{R} \underline{f}^j_{l\alpha_k} + \sum_{j=R+1}^{M} \overline{f}^j_{r\alpha_k}}\right]\left[\frac{1}{2} + \frac{\sqrt[2]{-2\ln(\alpha_k)}}{z}\right]\left[\sigma^i_{q\alpha_0}\right]\left[\frac{\left(x'_q - M^i_{q2\alpha_0}\right)^2}{\left[\left(\sigma^i_{x_{q2}}\right)^2 + \left(\sigma^i_{q\alpha_0}\right)^2\right]^2}\overline{f}^i_{r\alpha_0}\right]$
3	$x'_q \le \frac{M^i_{q1\alpha_0} + M^i_{q2\alpha_0}}{2} - \frac{\left(\sigma^i_{x_{q1}}\right)^2\left(M^i_{q2\alpha_0} - M^i_{q1\alpha_0}\right)}{2\left(\sigma^i_{q\alpha_0}\right)^2}$	$\underline{f}^i_{l\alpha_k} \in \left(\underline{f}^1_{l\alpha_k} \dots \underline{f}^R_{l\alpha_k}\right)$	$M^i_{q2\alpha_0}(new) = M^i_{q2\alpha_0}(now) + \frac{1}{2}K_{M_{q2\alpha_0}} e \sum_{k=0}^{2N+2} K_{\alpha_k}\left[\frac{\overline{c}^i_{r\alpha_k} - y_{r\alpha_k}}{\sum_{j=1}^{R} \underline{f}^i_{l\alpha_k} + \sum_{j=R+1}^{M} \overline{f}^i_{r\alpha_k}}\right]\left(\frac{1}{2} + \frac{\sqrt[2]{-2\ln(\alpha_k)}}{z}\right)\left[\left(\frac{x'_q - M^i_{q2\alpha_0}}{\left(\sigma^i_{x_{q1}}\right)^2 + \left(\sigma^i_q\right)^2}\right)\underline{f}^i_{l\alpha_0}\right]$

Preprints (www.preprints.org) | NOT PEER-REVIEWED | Posted: 31 October 2023 doi:10.20944/preprints202310.2072.v1

$$\sigma^i_{q\alpha_0}(new) = \sigma^i_{q\alpha_0}(now) + \frac{1}{2}K_{\sigma_q\alpha_0}e\sum_{k=0}^{2N+2}K_{\alpha_k}\left[\frac{\overline{c}^i_{r\alpha_k}-y_{r\alpha_k}}{\sum_{j=1}^{R}\underline{f}^j_{l\alpha_k}+\sum_{j=R+1}^{M}\overline{f}^j_{r\alpha_k}}\right]\left[\frac{1}{2}+\frac{\sqrt[2]{-2\,ln(\alpha_k)}}{z}\right]\left[\sigma^i_{q\alpha_0}\right]\left[\frac{\left(x'_q-M^i_{q2\alpha_0}\right)^2}{\left[\left(\sigma^i_{x_{q1}}\right)^2+\left(\sigma^i_{q\alpha_0}\right)^2\right]^2}\underline{f}^i_{l\alpha_0}\right]$$

4 x'_q $\underline{f}^i_{l\alpha_k}\in\left(\underline{f}^1_{l\alpha_k}\dots\underline{f}^R_{l\alpha_k}\right)$

$$\geq\frac{M^i_{q1\alpha_0}+M^i_{q2\alpha_0}}{2}+\frac{\left(\sigma^i_{x_{q1}}\right)^2\left(M^i_{q2\alpha_0}-M^i_{q1\alpha_0}\right)}{2\left(\sigma^i_{q\alpha_0}\right)^2}$$

$$M^i_{q1\alpha_0}(new) = M^i_{q1\alpha_0}(now) + \frac{1}{2}K_{M_{q1\alpha_0}}e\sum_{k=0}^{2N+2}K_{\alpha_k}\left[\frac{\overline{c}^i_{r\alpha_k}-y_{r\alpha_k}}{\sum_{j=1}^{R}\underline{f}^j_{l\alpha_k}+\sum_{j=R+1}^{M}\overline{f}^j_{r\alpha_k}}\right]\left[\frac{1}{2}+\frac{\sqrt[2]{-2\,ln(\alpha_k)}}{z}\right]\left[\left(\frac{x'_q-M^i_{q1\alpha_0}}{\left(\sigma^i_{x_{q1}}\right)^2+\left(\sigma^i_{q\alpha_0}\right)^2}\right)\underline{f}^i_{l\alpha_0}\right]$$

$$\sigma^i_{q\alpha_0}(new) = \sigma^i_{q\alpha_0}(now) + \frac{1}{2}K_{\sigma_q\alpha_0}e\sum_{k=0}^{2N+2}K_{\alpha_k}\left[\frac{\overline{c}^i_{r\alpha_k}-y_{r\alpha_k}}{\sum_{j=1}^{R}\underline{f}^j_{l\alpha_k}+\sum_{j=R+1}^{M}\overline{f}^j_{r\alpha_k}}\right]\left[\frac{1}{2}+\frac{\sqrt[2]{-2\,ln(\alpha_k)}}{z}\right]\left[\sigma^i_{q\alpha_0}\right]\left[\frac{\left(x'_q-M^i_{q1\alpha_0}\right)^2}{\left[\left(\sigma^i_{x_{q1}}\right)^2+\left(\sigma^i_{q\alpha_0}\right)^2\right]^2}\underline{f}^i_{l\alpha_0}\right]$$

2.3. The OLS Method for Consequent Tunning

Suppose that a particular system has one input $u(k)$ and one output $y(k)$ with an additive noise $e(k)$ measured t times every T period. Then it is possible to describe its dynamic behavior using the next model [125]:

$$y(k)=\sum_{j=1}^{n}a_j y(k-j)+\sum_{j=0}^{n}b_j u(k-j)+e(k) \quad (41)$$

Where $k=1,2,\dots t;\ a_j,\ b_j\ \ a_j\in R,\ n$ is the order of the system. This equation can be written in compact form:

$$y(k)=\boldsymbol{p}^T z(k)+e(k) \quad (42)$$

with $\boldsymbol{p}^T=[b_0,a_1,b_1,\dots,a_n,b_n]$ is the parameters estimation matrix of size $2n+1$ and $\boldsymbol{z}^T(k)=[u(k),y(k-1),u(k-1),\dots,y(k-n),u(k-n)]$ is the measurements vector. In the case of t input-output data pairs it can be expressed as:

$$\boldsymbol{Y}(t)=\boldsymbol{P^T Z}(t)+E(t) \quad (43)$$

with the output measured transpose vector of size

$$\boldsymbol{Y}^T(t)=[y(1),y(2),\dots,y(t)] \quad (44)$$

The measurements matrix can be expressed as:

$$\boldsymbol{Z}(t)=\begin{bmatrix} u(1), & u(2), & \cdots, & u(t)\\ y(0), & y(1), & \cdots, & y(t-1)\\ u(0), & u(1), & \cdots, & u(t-1)\\ \vdots & \vdots & \ddots & \vdots\\ y(1-n), & y(2-n), & \cdots, & y(t-n)\\ u(1-n), & y(2-n), & \cdots, & y(t-n)\end{bmatrix} \quad (45)$$

Preprints (www.preprints.org) | NOT PEER-REVIEWED | Posted: 31 October 2023 doi:10.20944/preprints202310.2072.v1

while the noise transpose vector as:

$$\boldsymbol{E}^T(t) = [e(1), e(2), \dots, e(t)] \tag{46}$$

It is required to minimize the next criteria during the estimation of P:

$$\boldsymbol{J} = (\boldsymbol{Y}(t) - \boldsymbol{Z}(t)\boldsymbol{P}(t))^T \boldsymbol{I}(\boldsymbol{Y}(t) - \boldsymbol{Z}(t)\boldsymbol{P}(t)) \tag{47}$$

with its least-squares solution as:

$$\widehat{\boldsymbol{P}}^T(t) = [\boldsymbol{Z}^T(t)\boldsymbol{Z}(t)]^{-1}\boldsymbol{Z}^T\boldsymbol{Y}(t) \tag{48}$$

On the other hand, the equation system

$$\boldsymbol{Ax} = \boldsymbol{b} \tag{49}$$

where $\boldsymbol{A}$ is a matrix of size $m\,x\,n$, $\boldsymbol{x}$ is a vector of size n, $\boldsymbol{b}$ is a vector of size m, with $m > n$. This system has a solution if b lies in the range space of A or equivalently $\rho(A) = \rho(A, b)$. Tacking a decomposition of b as $b = b_1 + e$, then (49) can be expressed as:

$$\boldsymbol{Ax} - b_1 = \boldsymbol{e} \tag{50}$$

Let's call $\boldsymbol{e}$ of size m the error. If

$$\boldsymbol{A}^T\boldsymbol{A} = \boldsymbol{F}^T\boldsymbol{F} \tag{51}$$

with $\boldsymbol{F}$ being any upper or lower triangular matrix of size n, then (49) can be written as:

$$\boldsymbol{F}^T\boldsymbol{Fx} = \boldsymbol{A}^T\boldsymbol{b_1} \tag{52}$$

A least-square solution can be found using previous equation (52). The method does not require the explicit factorization of $\boldsymbol{A}^T\boldsymbol{A}$ matrix nor the inverse matrix of $\boldsymbol{F}^T$. If the transformation matrix $\boldsymbol{F}$ is defined as:

$$\boldsymbol{F} = \begin{bmatrix} & & & j & & k & & \\ 1 & & & & & & & \\ & 1 & & & & & & \\ & & \ddots & & & & & \\ & & & c & & s & & \\ & & & -s & & c & & \\ & & & & & & \ddots & \\ & & & & & & & 1 \end{bmatrix} \tag{53}$$

It is easy to check that if the values of c and s are selected in such a way that the following condition is fulfilled:

$$c^2 + s^2 = 1 \tag{54}$$

Then the orthogonal transformation or rotational matrix can be defined as:

$$\boldsymbol{F}^T = \boldsymbol{F}^{-1} \tag{55}$$

which is known as rotational matrix because its application produces a rotation of an α angle in the system coordinates, with $\sin(\alpha) = c$ and $\cos(\alpha) = s$.

When an arbitrary $\boldsymbol{D}$ matrix is pre-multiplied by the $\boldsymbol{F}$ matrix, the rows j and k of the product will have the next values:

$$d'_j = cd_j + sd_k \tag{56}$$

$$d'_k = cd_k - sd_j \tag{57}$$

An adequate selection of c and s allows to override one element of the rows j or k. The successive application of m transformations of this type allow the cancellation of m row elements, finally obtaining the triangular matrix as result of successive transformations:

$$\Delta = \boldsymbol{F^m} \dots \boldsymbol{F'''F''F'D} = \boldsymbol{FD} \tag{58}$$

The rotational orthogonal transformations method is used to find the least-square solution of sub-determined systems of lineal equations.

Rewriting (50) as:

$$[\boldsymbol{A} \quad b_1]\begin{bmatrix} \boldsymbol{x} \\ -1 \end{bmatrix} = \boldsymbol{e} \tag{59}$$

Preprints (www.preprints.org) | NOT PEER-REVIEWED | Posted: 31 October 2023 doi:10.20944/preprints202310.2072.v1

If it is defined $\boldsymbol{D} = [\boldsymbol{A} \quad b_1]$ as a matrix of size $m\,x\,(n+1)$, and $\boldsymbol{x'} = \begin{bmatrix} \boldsymbol{x} \\ -1 \end{bmatrix}$ as a vector of size $(n+1)$ and applying the orthogonal transformation matrix $\boldsymbol{F}$ to (49), the next system is obtained:

$$\boldsymbol{FDx'} = \boldsymbol{Fe} \tag{60}$$

Then it is possible to apply the orthogonal transformation solution to the equation system (1) for its parameters identification. The last-square solution of (48) can be expressed as:

$$[\boldsymbol{Z}^T(t)\boldsymbol{Z}(t)]\boldsymbol{P}^T = \boldsymbol{Z}^T\boldsymbol{Y}(t) \tag{61}$$

The new estimation of the parameters $\boldsymbol{P}^T$ can be calculated by solving the triangular equivalent system:

$$\boldsymbol{F}(t)\boldsymbol{P}^T(t) = \boldsymbol{q}(t) \tag{62}$$

where the upper triangular matrix $\boldsymbol{F}(t)$ of size $2n+1$ is the square root of $\boldsymbol{Z}^T(t)\boldsymbol{Z}(t)$, and $\boldsymbol{q}(t)$ is a vector of size $2n+1$. The composition of $\boldsymbol{F}(t)$ and $\boldsymbol{q}(t)$ produces a triangular matrix 2n+2 represented in Figure 7.

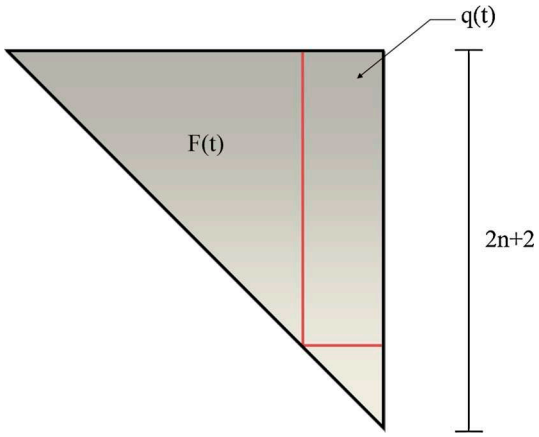

Figure 7. Schematic representation of **F**(*t*) and **q**(*t*), [125].

From the new measurements obtained at the time $(t+1)$ it is possible to create a new equation that has the form:

$$y(t+1) = \boldsymbol{z}^T(t+1)\boldsymbol{P}(t) \tag{63}$$

with

$$\boldsymbol{z}^T(t+1) = [u(t+1), y(t), u(t), \dots, y(t-n+1), u(t-n+1)] \tag{64}$$

The new system constituted by $\boldsymbol{F}(t)$, $\boldsymbol{q}(t)$ and $\boldsymbol{z}^T(t+1)$ as represented in Figure 8, can be reduced to a new triangular matrix to obtain by $\boldsymbol{F}(t+1)$ and $\boldsymbol{q}(t+1)$. For each period, the previous algorithm reduces to zero the compound vector $[\boldsymbol{z}^T(t+1), y(t+1)]$, of size $2n+2$, to calculate $\boldsymbol{F}(t+1)$ and $\boldsymbol{q}(t+1)$, as represented in Figure 9. Then the parameters of $\widehat{\boldsymbol{P}}^T(t+1)$ can be calculated by solving the triangular equivalent system of (1)

$$\boldsymbol{F}(t+1)\widehat{\boldsymbol{P}}^T(t+1) = \boldsymbol{q}(t+1) \tag{65}$$

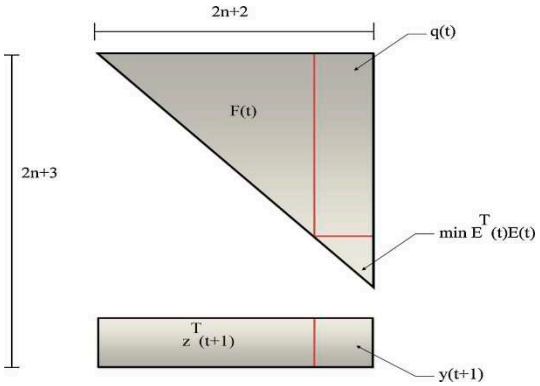

Figure 8. ^{T} (*t*+1), [125].

Preprints (www.preprints.org) | NOT PEER-REVIEWED | Posted: 31 October 2023 doi:10.20944/preprints202310.2072.v1

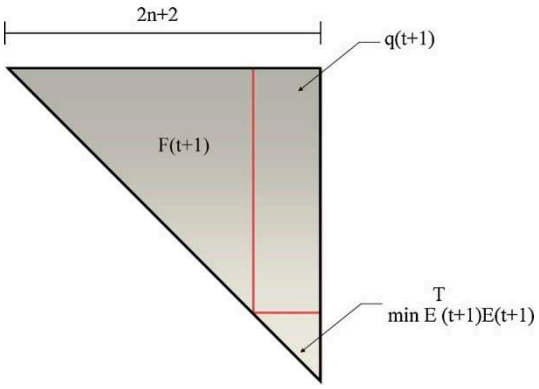

Figure 9. Schematic representation of F(*t*+1) and q(*t*+1), [125].

$$\widehat{\boldsymbol{P}}^{T}(t+1) = \boldsymbol{F}^{-1}(t+1)\boldsymbol{q}(t+1) \tag{66}$$

Considering

$$y_{l\alpha_k} = \frac{\sum_{n=1}^{L} \overline{f}^{n}_{\alpha_k} * c^{n}_{l\alpha_k} + \sum_{n=L+1}^{M} \underline{f}^{n}_{\alpha_k} * c^{n}_{l\alpha_k}}{\sum_{n=1}^{L} \overline{f}^{n}_{\alpha_k} + \sum_{n=L+1}^{M} \underline{f}^{n}_{\alpha_k}} \tag{67}$$

$$y_{r\alpha_k} = \frac{\sum_{n=1}^{R} \underline{f}^{n}_{\alpha_k} * c^{n}_{r\alpha_k} + \sum_{n=R+1}^{M} \overline{f}^{n}_{\alpha_k} * c^{n}_{r\alpha_k}}{\sum_{n=1}^{R} \underline{f}^{n}_{\alpha_k} + \sum_{n=R+1}^{M} \overline{f}^{n}_{\alpha_k}} \tag{68}$$

$$\boldsymbol{\lambda}_{l\alpha_k} = \left[\overline{f}^{1}_{\alpha_k}, \overline{f}^{2}_{\alpha_k} \ldots \overline{f}^{L}_{\alpha_k}, \underline{f}^{L+1}_{\alpha_k}, \underline{f}^{L+2}_{\alpha_k}, \ldots \underline{f}^{M}_{\alpha_k}\right]^{T} \tag{69}$$

$$\boldsymbol{\lambda}_{r\alpha_k} = \left[\underline{f}^{1}_{\alpha_k}, \underline{f}^{2}_{\alpha_k} \ldots \underline{f}^{R}_{\alpha_k}, \overline{f}^{R+1}_{\alpha_k}, \overline{f}^{R+2}_{\alpha_k}, \ldots \overline{f}^{M}_{\alpha_k}\right]^{T} \tag{70}$$

and

$$\boldsymbol{\theta}_{l\alpha_k} = \left[\underline{c}^{1}_{l\alpha_k}, \underline{c}^{2}_{l\alpha_k}, \ldots \underline{c}^{M}_{l\alpha_k}\right]^{T} \tag{71}$$

$$\boldsymbol{\theta}_{r\alpha_k} = \left[\overline{c}^{1}_{r\alpha_k}, \overline{c}^{2}_{r\alpha_k}, \ldots \overline{c}^{M}_{r\alpha_k}\right]^{T} \tag{72}$$

Then

$$\boldsymbol{y}_{l\alpha_k} = \boldsymbol{\lambda}^{T}_{l\alpha_k}\boldsymbol{\theta}_{l\alpha_k} \tag{73}$$

$$\boldsymbol{y}_{r\alpha_k} = \boldsymbol{\lambda}^{T}_{r\alpha_k}\boldsymbol{\theta}_{r\alpha_k} \tag{74}$$

The OLS method, [125], can be used recursively online, starting with the next initial conditions: $\boldsymbol{F_l}(0) = \boldsymbol{\lambda}_{l\alpha_0}$, $\boldsymbol{P_l}(0) = \boldsymbol{\theta}_{l\alpha_0}$, $\boldsymbol{q_l}(0) = y$, $\boldsymbol{F_r}(0) = \boldsymbol{\lambda}_{r\alpha_0}$, $\boldsymbol{P_r}(0) = \boldsymbol{\theta}_{r\alpha_0}$ and $\boldsymbol{q_r}(0) = y$, where y is the output value of the training input-output data pair. The pseudocode of the OLS is shown in Algorithm 1.

Algorithm 1:	Parameter estimation using rotational orthogonal transformation
1:	**Initialize** n, $\boldsymbol{F_l}(0) = \boldsymbol{\lambda}_{l\alpha_0}$, $\boldsymbol{P_l}(0) = \boldsymbol{\theta}_{l\alpha_0}$, $\boldsymbol{q_l}(0) = y$, $\boldsymbol{F_r}(0) = \boldsymbol{\lambda}_{r\alpha_0}$, $\boldsymbol{P_r}(0) = \boldsymbol{\theta}_{r\alpha_0}$ and $\boldsymbol{q_r}(0) = y$
2:	**Triangulate** the $\boldsymbol{F_l}$ and $\boldsymbol{F_r}$ matrices
3:	**Solve** the equations system. $\widehat{\boldsymbol{P}}^{T}_{\boldsymbol{l}}(t+1) = \boldsymbol{F_l}^{-1}(t+1)\boldsymbol{q_l}(t+1)$ and $\widehat{\boldsymbol{P}}^{T}_{\boldsymbol{r}}(t+1) = \boldsymbol{F_r}^{-1}(t+1)\boldsymbol{q_r}(t+1)$
4:	**Assign** estimated values. $\widehat{\boldsymbol{\theta}}_{l\alpha_0} = \widehat{\boldsymbol{P}}_{\boldsymbol{l}}(t+1)$, $\widehat{\boldsymbol{\theta}}_{r\alpha_0} = \widehat{\boldsymbol{P}}_{\boldsymbol{r}}(t+1)$

Preprints (www.preprints.org) | NOT PEER-REVIEWED | Posted: 31 October 2023 doi:10.20944/preprints202310.2072.v1

3. Results and Discussion

3.1. The Problem: Industrial Process Description

The HSM process presents many complexities and uncertainties involved in rolling operations. Figure 10 shows the HSM sub-processes: The reheat furnace, the roughing mill (RM), the transfer tables, the scale breaker (SB), the finishing mill (FM), the round out tables, and the coiler (CLR).

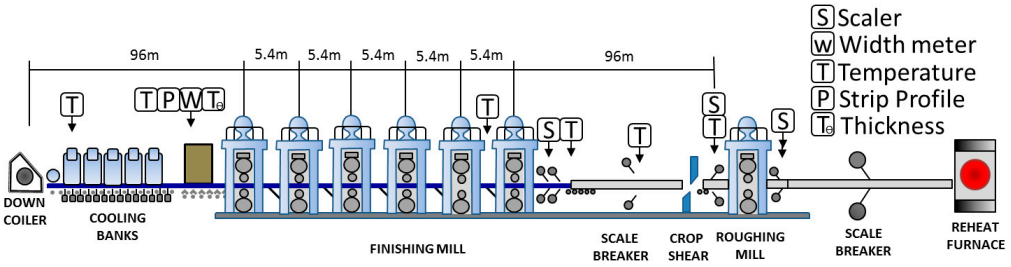

Figure 10. Schematic representation of HSM, [5].

The most critical subprocess is the FM. There are several mathematical model-based systems for setting up the FM, which calculate the working references required to obtain the target strip gauge, target strip width and target strip temperature at the exit zone of the FM. The math model takes as inputs the FM target strip gage, the target strip width, the target strip temperature, the slab steel grade, the hardness ratio from slab chemistry, the FM load distribution, the FM gauge offset, the FM temperature offset, the FM roll diameters, the FM load distribution, the input transfer bar gauge, the input transfer bar width, and the most critical variable, the input transfer bar temperature.

The math model requires knowing accurately what the input transfer bar temperature is at the entry zone of the FM. A minimum entry temperature error will propagate through the entire FM and produce a coil out of the required quality. For the estimation of this FM entry temperature, the math models require knowledge of the transfer bar surface temperature, which is measured by a pyrometer located at the RM exit side, and knowledge of the time taken to translate the transfer bar from the RM exit zone to the FM SB entry zone.

These pyrometer's measurements are affected by the noise produced by the surface scale growth, environment water steam, the pyrometer's location, calibration, resolution, repeatability, and by the recalescence phenomenon occurring at the RM exit in the body of the transfer bar [126]. The time required by the transfer bar to move its head end from the RM exit to the FM entry zones, is estimated by the math model. This time estimation is affected by the free air radiation phenomenon occurring during the transfer bar translation and by the inherent uncertainty of the kinematic and dynamic modeling.

The math model parameters are adjusted using both the uncertain surface temperature measured by pyrometers located at the FM entry zone, and the uncertain surface temperature at the FM entry zone estimated by the model. The proposal estimates the input transfer bar temperature at the entry zone of the FM and was off-line tested using real data from an industrial HSM facility located in Monterrey, México, which is currently using a certain type of fuzzy system for this estimation.

3.2. Simulation

This section presents the experimental testing of the proposal, the prediction of the transfer bar surface temperature.

3.2.1. Input-output Data Pairs

From an industrial HSM process, one hundred and seventy-five noisy input-output data pairs of three different types of coils, Table 7, were obtained and used as offline training data, (x_1', x_2', y). The inputs were x_1', the transfer bar surface temperature measured by the pyrometer is located at the RM exit zone, and x_2', the real time to move the transfer bar end from the RM exit zone to the SB

Preprints (www.preprints.org) | NOT PEER-REVIEWED | Posted: 31 October 2023 doi:10.20944/preprints202310.2072.v1

entry zone. The output y was the transfer bar surface temperature measured by the pyrometers located at the SB entry zone and used to calculate the temperature prediction error.

Table 7. Type of coils.

Coil type	Target gage (mm)	Target width (mm)	Steel grade (SAE-AISI)
A	1.879	1041.0	1006
B	2.006	991.0	1006
C	2.159	952.0	1006

3.2.2. Antecedent Membership Functions

The primary membership functions for each antecedent of the base IT2α_0 NSFLS-2 system were Gaussian functions with uncertain means $M^i_{q1\alpha_0}$, $M^i_{q2\alpha_0}$, and with the standard deviation $\sigma^i_{q\alpha_0}$, as shown in Tables 8 and 9. An array of two inputs, with five MF each, produces $M = 25$ rules.

Table 8. Parameters for MFs of x'_1.

	$M^i_{11\alpha_0}$ (℃)	$M^i_{12\alpha_0}$ (℃)	$\sigma^i_{1\alpha_0}$ (℃)
1	1010	1012	30
2	1040	1042	30
3	1070	1072	30
4	1100	1102	30
5	1130	1132	30

Table 9. Parameters for MFs of x'_2.

	$M^i_{21\alpha_0}$ (s)	$M^i_{22\alpha_0}$ (s)	$\sigma^i_{2\alpha_0}$ (s)
1	32.16	32.66	2.72
2	34.88	35.38	2.72
3	37.60	38.10	2.72
4	40.32	40.82	2.72
5	43.04	43.54	2.72

3.2.3. Fuzzy Rule Base

The EWH IT3 NSFLS-1 fuzzy rule base consists of a set of IF-THEN rules that represent the model of the complete system. The IT2α_0 NSFLS-1, that is the base of the 3D construction of the proposed fuzzy system, has two inputs x'_1 and x'_2 and one output y_α. The rule base has $M = 25$ rules of the type shown in Table 10.

Table 10. Initial fuzzy rule base.

Rule	$M^i_{12\alpha_0}$ (℃)	$M^i_{12\alpha_0}$ (℃)	$\sigma^i_{1\alpha_0}$ (℃)	$M^i_{21\alpha_0}$ (s)	$M^i_{22\alpha_0}$ (s)	$\sigma^i_{2\alpha_0}$ (s)	$\underline{c}^i_{l\alpha_0}$ (℃)	$\overline{\sigma}^i_{r\alpha_0}$ (℃)
1	1010	1012	30	32.16	32.66	2.7	960	962
2	1010	1012	30	34.88	35.38	2.7	958	960

Preprints (www.preprints.org) | NOT PEER-REVIEWED | Posted: 31 October 2023 doi:10.20944/preprints202310.2072.v1

3	1010	1012	30	37.60	38.10	2.7	956	958
4	1010	1012	30	40.32	40.82	2.7	954	956
5	1010	1012	30	43.04	43.54	2.7	952	954
6	1040	1042	30	32.16	32.66	2.7	970	972
7	1040	1042	30	34.88	35.38	2.7	968	970
8	1040	1042	30	37.60	38.10	2.7	966	968
9	1040	1042	30	40.32	40.82	2.7	964	966
10	1040	1042	30	43.04	43.54	2.7	962	964
11	1070	1072	30	32.16	32.66	2.7	980	982
12	1070	1072	30	34.88	35.38	2.7	978	980
13	1070	1072	30	37.60	38.10	2.7	976	978
14	1070	1072	30	40.32	40.82	2.7	974	976
15	1070	1072	30	43.04	43.54	2.7	972	974
16	1100	1102	30	32.16	32.66	2.7	990	992
17	1100	1102	30	34.88	35.38	2.7	988	990
18	1100	1102	30	37.60	38.10	2.7	986	988
19	1100	1102	30	40.32	40.82	2.7	984	986
20	1100	1102	30	43.04	43.54	2.7	982	984
21	1130	1132	30	32.16	32.66	2.7	1000	1002
22	1130	1132	30	34.88	35.38	2.7	998	1000
23	1130	1132	30	37.60	38.10	2.7	996	998
24	1130	1132	30	40.32	40.82	2.7	994	996
25	1130	1132	30	43.04	43.54	2.7	992	994

3.3. Results and Discusion

Three different sets of data for three different coil types were taken from a real mill. Each of these data sets was split into two sets: One for the initial adjustment and tuning process, and the other for the setup validation process. Eighty-three of type A, sixty-five of type B and twenty-seven of type C input-output data pairs were used for the initial offline training process, and seven input-output data pairs were used for testing. The production gage and width coil targets of the training data with the steel grade are shown in Table 7. A Dell PC i7, 16 GB RAM memory and 2.8 GHz using Win 11 OS was used to execute the fuzzy systems programed in MS VS 2022 C++ language.

Seven input-output data pairs were used to test the offline SB entry temperature estimation. The Root Mean Square Error (RMSE) for the prediction obtained with GT2 models trained with the BP-BP algorithm and IT2 systems used as benchmark models and the proposed EWH algorithm with BP-BP using only one α_k-cuts are shown in Table 11 and Figure 11. The EWH algorithm shows an enhancement of 0.2 % versus the classic WH model using BP-BP learning model for the GT2 SFLS systems. On other hand, the WH algorithm using IT3 SFLS models show an enhancement of 0.36% for classic WH singleton and 0.41% the EWH proposed algorithm in singleton compared with the IT2 singleton model as shown in Table 12 and Figure 12.

For non-singleton cases, both models, WH and EWH, present the same prediction in the case of the GT2 models. In contrast the IT3 models show a bigger enhancement versus the IT2 NSFLS-1 models. In the first case the WH IT3 NSFLS-1 (BP-BP) show an enhancement of 22.5 % for the WH algorithm and 30.2% for the EWH proposed algorithm as shown in Table 12 and Figure 12.

Table 11. Comparison between the benchmark models (IT2 SFLS and IT2 NSFLS-1) and GT2 models with BP-BP learning using the classic WH algorithm and the EWH algorithm.

Preprints (www.preprints.org) | NOT PEER-REVIEWED | Posted: 31 October 2023 doi:10.20944/preprints202310.2072.v1

Fuzzy System\ α_k-cuts	1
IT2 SFLS	1.4249
IT2 NSFLS-1	1.2542
WH GT2 SFLS (BP-BP)	1.4515
EWH GT2 SFLS (BP-BP)	1.4497
WH GT2 NSFLS-1 (BP-BP)	1.0383
EWH GT2 NSFLS-1 (BP-BP)	1.0383

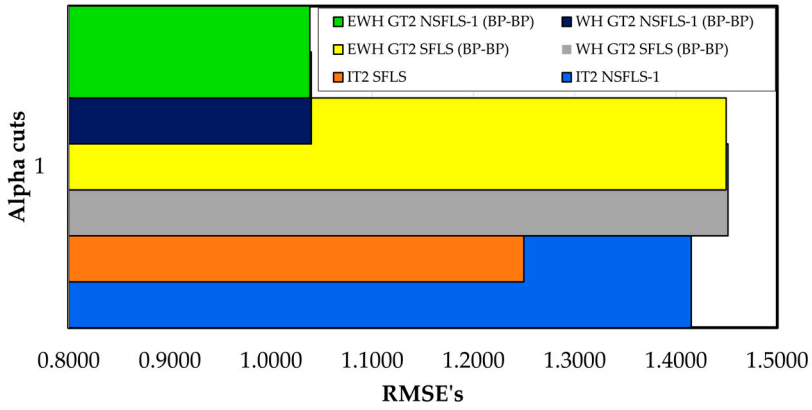

Figure 11. RMSE of prediction of GT2 systems with BP-BP learning.

Table 12. Comparison between the benchmark models (IT2 SFLS and IT2 NSFLS-1) and IT3 models with BP-BP learning using the classic WH algorithm and the EWH algorithm.

Fuzzy System\ α_k-cuts	1	2
IT2 SFLS	1.4249	
IT2 NSFLS-1	1.2542	
WH IT3 SFLS (BP-BP)		1.4212
EWH IT3 SFLS (BP-BP)		1.4192
WH IT3 NSFLS-1 (BP-BP)		0.9729
EWH IT3 NSFLS-1 (BP-BP)		0.8761

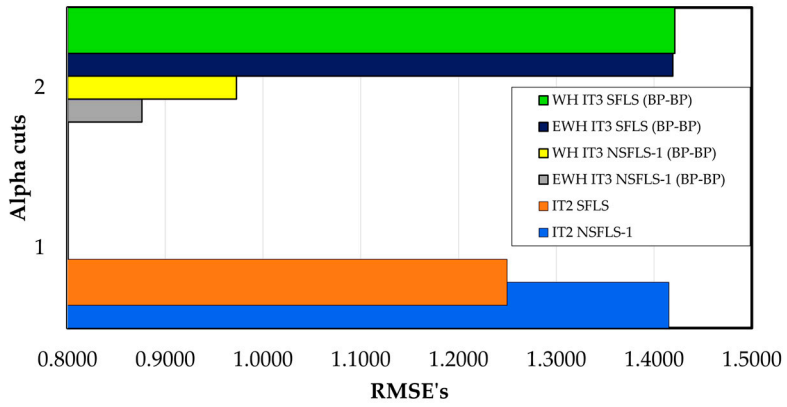

Figure 12. RMSE of prediction of IT3 systems with BP-BP learning.

The RMSE prediction of the GT2 and the proposed EWH algorithm using different levels-α_k as shown in Table 13 and Figure 13, show that the GT2 SFLS-1 (BP-BP) with the proposed model (EWH)

Preprints (www.preprints.org) | NOT PEER-REVIEWED | Posted: 31 October 2023 doi:10.20944/preprints202310.2072.v1

outperforms the WH GT2 SFLS with only 10 α_k-cuts in an order of 19.1% for WH GT2 singleton with BP-BP learning algorithm and 19.5% for the IT3 with the EWH algorithm with BP-BP learning as is shown in Table 14. On other hand, with the non-singleton models the enhancement is 2.3% for the WH algorithm and 17% for the EWH algorithm for both with BP-BP learning. The best results are obtained with 100 α_k-cuts with an enhancement of 12.3% for the WH algorithm and 17.5% for the EWH algorithm, both with BP-BP learning as shown in Table 13 and Figure 13.

Table 13. Comparison between the benchmark models (IT2 SFLS and IT2 NSFLS-1) and GT2 models with BP-BP learning using the classic WH algorithm and the EWH algorithm with different number of α_k-cuts.

Fuzzy System\ α_k-cuts	1	10	100	1000
IT2 SFLS	1.4249			
IT2 NSFLS-1	1.2542			
WH GT2 SFLS (BP-BP)	1.4515	1.1501	1.4912	1.5727
EWH GT2 SFLS (BP-BP)	1.4497	1.1433	1.4852	1.5166
WH GT2 NSFLS-1 (BP-BP)	1.0397	1.2338	1.097	1.3325
EWH GT2 NSFLS-1 (BP-BP)	1.0383	1.1534	1.0321	1.326

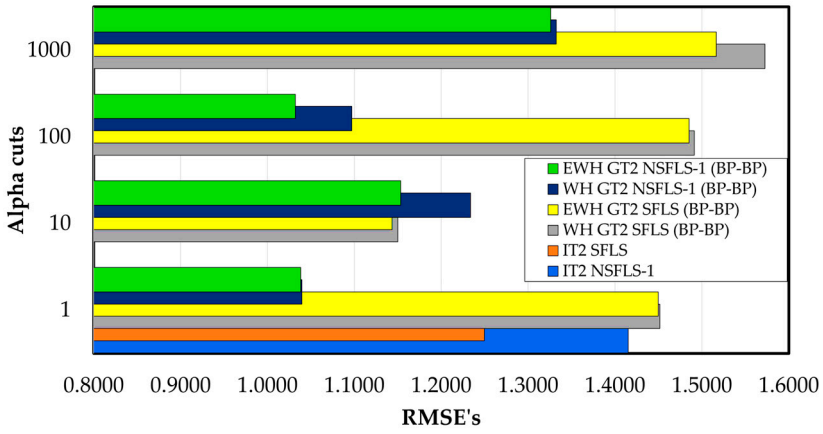

Figure 13. RMSE of prediction of GT2 systems with BP-BP learning.

In contrast when the IT3 fuzzy systems are used the results show a reduction in the error rates in every number of α_k-cuts tested. E.g., with 202 α_k-cuts the enhancement versus the IT2 SFLS using the WH learning is in the order of 1.4%, and for the EWH IT3 NSFLS-1 (BP-BP) is in the order of 27.9% as it is shown in Table 14 and Figure 14.

Table 14. Comparison between the benchmark models (IT2 SFLS and IT2 NSFLS-1) and IT3 models with BP-BP learning using the classic WH algorithm and the EWH algorithm with different number of α_k-cuts.

Fuzzy System\ α_k-cuts	1	2	22	202	2002
IT2 SFLS	1.4249				
IT2 NSFLS-1	1.2542				
WH IT3 SFLS (BP-BP)		1.4212	1.0573	1.4063	1.4568
EWH IT3 SFLS (BP-BP)		1.4192	1.0528	1.4016	1.4239
WH IT3 NSFLS-1 (BP-BP)		0.9729	1.1107	1.0547	1.2197
EWH IT3 NSFLS-1 (BP-BP)		0.8761	1.0125	1.0275	1.168

Preprints (www.preprints.org) | NOT PEER-REVIEWED | Posted: 31 October 2023 doi:10.20944/preprints202310.2072.v1

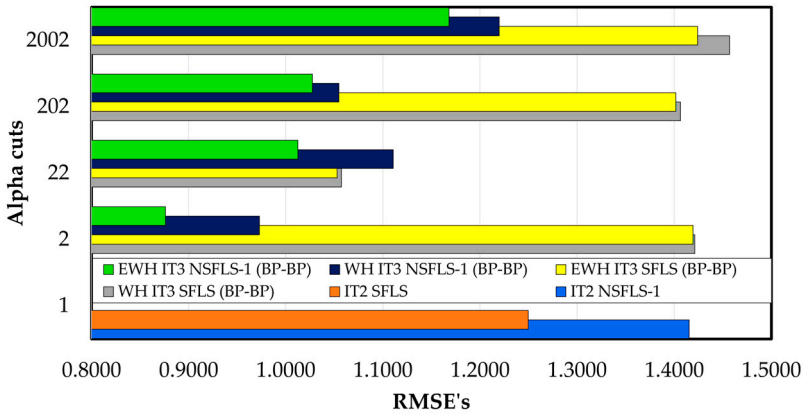

Figure 14. RMSE of prediction of IT3 systems with BP-BP learning.

The values of the RMSE of the GT2 using the proposed hybrid learning (OLS-BP) with the WH and the proposed EWH are presented in Table 15 for only 1 α_k-cut. Their results show an enhancement of 34.2 % comparing the IT2 SFLS with the WH GT2 SFLS using OLS-BP learning and shows an enhancement of 33.9 % when comparing the IT2 SFLS against EWH GT2 SFLS (OLS-BP) system (see Table 15, and Figure 15). The results show that the tested systems WH GT2 SFLS (OLS-BP) and the EWH GT2 SLFS (OLS-BP) outperforms the IT2 SFLS with only 1 α_k-cut. In a complementary form the WH GT2 NSFLS-1 (OLS-BP) presents an enhancement of 28.7% for the WH GT2 NSFLS-1 (OLS-BP) learning and 30.5% for the EWH GT2 NSFLS-1 (OLS-BP) system.

Table 15. Comparison between the benchmark models (IT2 SFLS and IT2 NSFLS-1) and GT2 models with OLS-BP learning using the classic WH algorithm and the EWH algorithm.

Fuzzy System\ α_k-cuts	1
IT2 SFLS	1.4249
IT2 NSFLS-1	1.2542
WH GT2 SFLS (OLS-BP)	0.9389
EWH GT2 SFLS (OLS-BP)	0.9424
WH GT2 NSFLS-1 (OLS-BP)	0.8952
EWH GT2 NSFLS-1 (OLS-BP)	0.8724

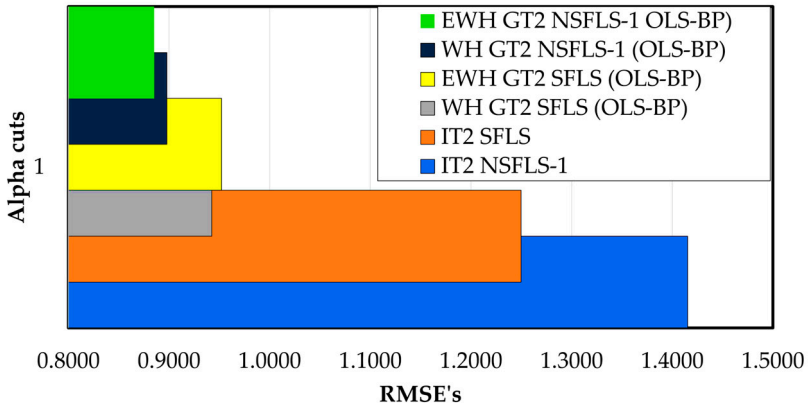

Figure 15. RMSE of prediction of GT2 systems with OLS-BP learning.

Preprints (www.preprints.org) | NOT PEER-REVIEWED | Posted: 31 October 2023 doi:10.20944/preprints202310.2072.v1

On other hand, the RMSE for the prediction using both the WH and the EWH IT3 models with the OLS-BP learning algorithms, shows that the error rates are reduced significantly to 34.2% for the WH IT3 SFLS (OLS-BP), 33.9% for the EWH algorithm in the IT3 SFLS (OLS-BP) as shown in Table 16 and Figure 16. For the IT3 with only two α_k-cuts the IT3 NSFLS-1 model presents continuous enhancements when compared with IT2 and with GT2 systems. The WH IT3 NSFLS-1 (OLS-BP) system presents better performance with a reduction of 28.7% and 30.5% for the EWH IT3 NSFLS-1 (OLS-BP) model, as shown in Table 16 and Figure 16.

Table 16. Comparison between the benchmark models (IT2 SFLS and IT2 NSFLS-1) and IT3 models with OLS-BP learning using the classic WH algorithm and the EWH algorithm.

Fuzzy Systems\ α_k-cuts	1	2
IT2 SFLS	1.4249	
IT2 NSFLS-1	1.2542	
WH IT3 SFLS (OLS-BP)		0.9389
EWH IT3 SFLS (OLS-BP)		0.9424
WH IT3 NSFLS-1 (OLS-BP)		0.8952
EWH IT3 NSFLS-1 (OLS-BP)		0.8724

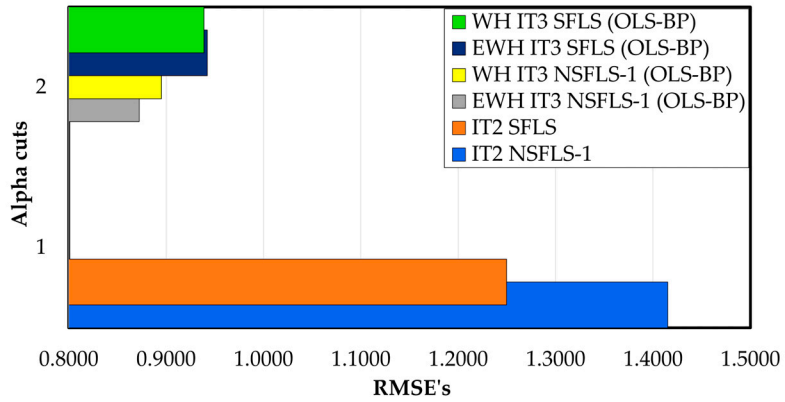

Figure 16. RMSE of prediction of IT3 systems with OLS-BP learning.

Table 17 shows the RMSE of the GT2 systems using the OLS-BP learning algorithm with different number of α_k-cuts. The results show a significant reduction versus the IT2 SFLS systems presenting a 34.2% in the comparison against WH GT2 SFLS (OLS-BP) learning and 33.9% against IT2 SFLS and for 33.2% for EWH GT2 SFLS (OLS-BP) system. In contrast, when comparing the non-singleton models it is obtained 38.5 % and 29.5 % for the WH GT2 NSFLS-1 (OLS-BP) and EWH GT2 NSFLS1 (OLS-BP), respectively. In a complementary form the WH GT2 NSFLS-1 (OLS-BP) presents an enhancement of 28.7% for the WH GT2 NSFLS-1 (OLS-BP) learning and 30.5% for the EWH GT2 NSFLS-1 (OLS-BP) system. Compared with the IT3 models, the RMSE showed a reduction on the error of prediction of 34.2% for WH IT3 SFLS (OLS-BP), 33.9% for EWH IT3 SLFS (OLS-BP) models. For non-singleton models a reduction of 38.7% for the IT3 NSFLS-1 (OLS-BP) and 30.15% against the IT2 NSFLS-1 were obtained, respectively.

Table 17. Comparison between the benchmark models (IT2 SFLS and IT2 NSFLS-1) and GT2 models with OLS-BP learning using the classic WH algorithm and the EWH algorithm.

Fuzzy System\ α_k-cuts	1	10	100	1000
IT2 SFLS	1.4249			
IT2 NSFLS-1	1.2542			

Preprints (www.preprints.org) | NOT PEER-REVIEWED | Posted: 31 October 2023 doi:10.20944/preprints202310.2072.v1

WH GT2 SFLS (OLS-BP)	0.9424	0.9332	0.9356	0.9631
EWH GT2 SFLS (OLS-BP)	0.9521	0.9438	0.9458	0.9658
WH GT2 NSFLS-1 (OLS-BP)	0.8979	0.9316	0.8888	1.002
EWH GT2 NSFLS1 (OLS-BP)	0.8851	0.9183	0.8659	0.9967

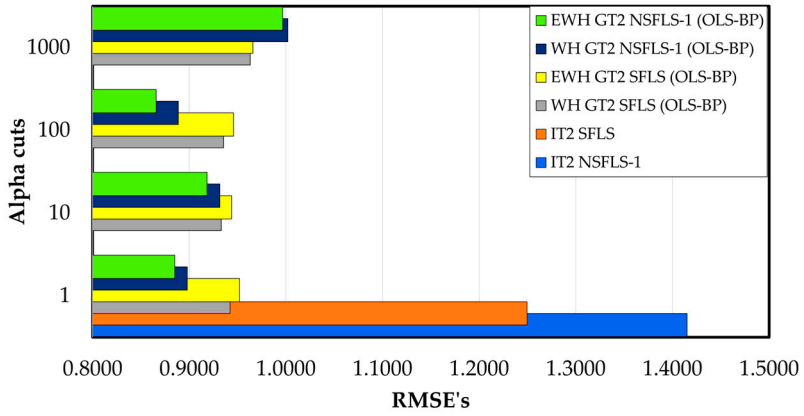

Figure 17. RMSE of prediction of GT2 systems with OLS-BP learning.

The values of RMSE prediction for the IT3 using the proposed learning OLS-BP with the WH algorithm and the proposed EWH algorithm are presented in Table 18 using different quantities of α_k-cuts. The results show an enhancement of 34.2 % comparing the IT2 SFLS with the WH IT3 SFLS algorithm using OLS-BP learning. It also showed an enhancement of 33.9 % comparing the IT2 SFLS to the EWH IT3 SFLS (OLS-BP) system as shown in Table 18 and Figure 18, demonstrating that the tested systems WH IT3 SFLS (OLS-BP) and EWH IT3 SLFS (OLS-BP) outperforms the IT2 SFLS with only 2 α_k-cuts.

Table 18. Comparison between the benchmark models (IT2 SFLS and IT2 NSFLS-1) and IT3 models with OLS-BP learning using the classic WH algorithm and the EWH algorithm.

Fuzzy System\ α_k-cuts	**1**	**2**	**10**	**100**	**1000**
IT2 SFLS	1.4249				
IT2 NSFLS-1	1.2542				
WH IT3 SFLS (OLS-BP)		0.9389	0.9247	0.9177	0.9461
EWH IT3 SFLS (OLS-BP)		0.9424	0.9184	0.9231	0.9556
WH IT3 NSFLS-1 (OLS-BP)		0.8952	0.9127	0.8795	0.9666
EWH IT3 NSFLS-1 (OLS-BP)		0.8724	0.8905	0.8634	0.9408

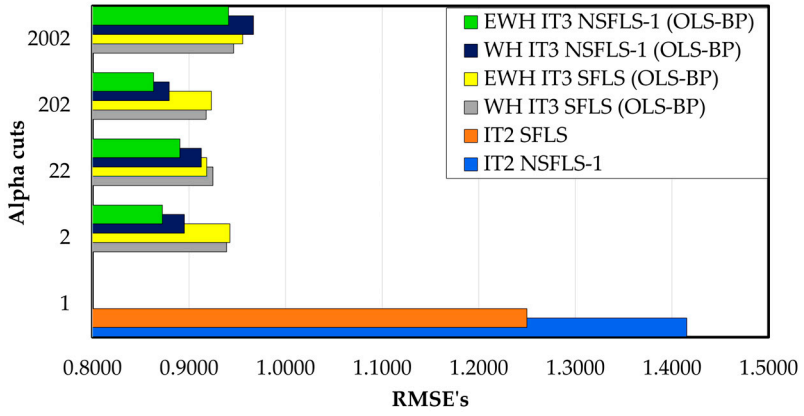

Preprints (www.preprints.org) | NOT PEER-REVIEWED | Posted: 31 October 2023 doi:10.20944/preprints202310.2072.v1

Figure 18. RMSE of prediction of IT3 systems with OLS-BP learning.

For offline tuning, twenty training epochs were used with validated and bounded input-output data pairs, which guarantees the convergence of the proposed EWH IT3 NSFLS-1, as experimentally demonstrated in this research.

With the proposed OLS-BP hybrid training method, the IT3 NSFLS-1 was the one that presented the best performance. The results obtained by the GT2 systems are better than the IT2 models but, however, not better than the IT3 systems as shown in Figure 19.

The results show that the best estimation is obtained by the proposed EWH IT3 NSFLS-1 (OLS-BP) model using 202 levels-α with a RMSE = 0.8634°C. The IT3 NSFLS-1 using any number of levels-α presented the values of RMSE below to 1°C as shown in Figure 20.

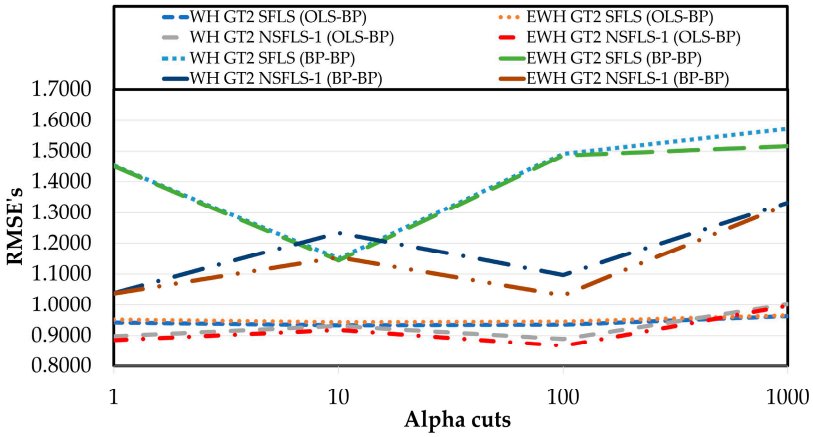

Figure 19. RMSE of prediction of GT2 systems with OLS-BP learning.

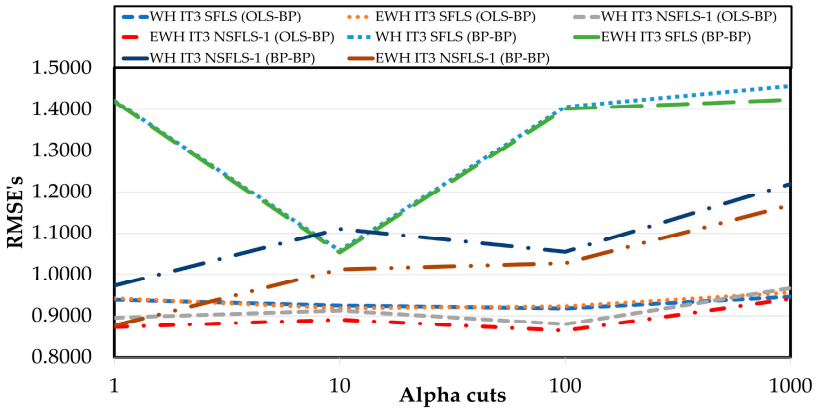

Figure 20. RMSE of prediction of IT3 systems with OLS-BP learning.

4. Conclusions

This work presents a novel hybrid learning method for parameter tuning of the novel EWH method for IT3 NSFLS-1 output estimation. The consequent parameters are tuned using the OLS training algorithm, while the antecedent parameters are tuned using the classic BP algorithm. The proposed EWH fuzzy systems use the average instead of the weighted average, to estimate the final output value of the fuzzy system, y_{α}, where the contribution of the horizontal level-α_0 or IT2α_0 FLS output, y_{α_0}, improves the accuracy of this estimation. Each horizontal level-α_k contributes 100% with its estimation of its output, y_{α_k}.

The simulation results show that the proposed EWH IT3 NSFLS-1 (OLS-BP) hybrid algorithm produces better performance to generate better temperature estimation when compared with the BP-BP training. The better performance is obtained by the proposed EWH fuzzy systems when compared

Preprints (www.preprints.org) | NOT PEER-REVIEWED | Posted: 31 October 2023 doi:10.20944/preprints202310.2072.v1

with the classic WH fuzzy systems. Also, the comparisons between several types of fuzzy systems showed that the IT3 NSFLS-1 are the best among the IT3 SFLS, GT2 NSFLS-1, GT2 SFLS, and the IT2 fuzzy systems.

For the future work, we plan to apply the hybrid algorithm and the EWH to the GT2 fuzzy systems and apply this system to FM exit gage, FM exit width, and FM exit temperature estimation of the head strip.

Author Contributions: For research articles with several authors, a short paragraph specifying their individual contributions must be provided. The following statements should be used "Conceptualization, Gerardo Mendez; Data curation, Gerardo Mendez, Ismael Lopez Juarez, Maria Alcorta Garcia and Pascual Montes Dorantes; Formal analysis, Gerardo Mendez, Ismael Lopez Juarez, Maria Alcorta Garcia, Dulce Martinez Peon and Pascual Montes Dorantes; Investigation, Gerardo Mendez, Maria Alcorta Garcia, Dulce Martinez Peon and Pascual Montes Dorantes; Methodology, Gerardo Mendez and Pascual Montes Dorantes; Project administration, Gerardo Mendez; Resources, Gerardo Mendez, Ismael Lopez Juarez, Maria Alcorta Garcia, Dulce Martinez Peon and Pascual Montes Dorantes; Software, Gerardo Mendez and Pascual Montes Dorantes; Validation, Gerardo Mendez, Ismael Lopez Juarez, Maria Alcorta Garcia, Dulce Martinez Peon and Pascual Montes Dorantes; Visualization, Gerardo Mendez, Ismael Lopez Juarez, Maria Alcorta Garcia, Dulce Martinez Peon and Pascual Montes Dorantes; Writing – original draft, Gerardo Mendez and Pascual Montes Dorantes; Writing – review & editing, Gerardo Mendez, Ismael Lopez Juarez, Maria Alcorta Garcia, Dulce Martinez Peon and Pascual Montes Dorantes. All authors have read and agreed to the published version of the manuscript.".

Funding: This research received no external funding.

Conflicts of Interest: The authors declare no conflict of interest.

References

1. Castillo, O; Castro, J.R.; Melin, P. Interval type-3 fuzzy fractal approach in sound speaker quality control evaluation. *Eng. Appl. Artif. Intell.* **2022**, 116, 105363. https://doi.org/10.1016/j.engappai.2022.105363.
2. Castillo, O.; Castro, J.R.; Melin, P. Interval Type-3 Fuzzy Systems: Theory and Design. Studies in Fuzziness and Soft Computing, 418 1st ed. Springer Nature: Switzerland, 2022; pp. 1-100. https://doi.org/10.1007/978-3-030-96515-0.
3. Castillo, O.; Melin, P. Towards interval type-3 intuitionistic fuzzy sets and systems. *Mathematics* **2022**, 10, 21, 4091. https://doi.org/10.3390/math10214091.
4. Peraza, C.; Ochoa, P.; Castillo, O.; Geem, Z.W. Interval type-3 fuzzy differential evolution for designing an interval type-3 fuzzy controller of a unicycle mobile robot. *Mathematics* **2022**, 10, 19, 3533. https://doi.org/10.3390/math10193533.
5. Méndez, G.M.; Lopez-Juarez, I.; Dorantes, P.N.M.; Alcorta M. A. A New method for design of interval type-3 fuzzy logic systems with uncertain type-2 non-singleton inputs (IT3 NSFLS-2): A study case in a hot strip mill. *IEEE Access* **2023**, 11, 44065-44081. DOI. 10.1109/ACCESS.2023.3272531.
6. Amador-Angulo, L.; Castillo, O.; Melin, P.; Castro, J. R. Interval type-3 fuzzy adaptation of the bee colony optimization algorithm for optimal fuzzy control of an autonomous mobile robot. *Micromachines* **2022**, 13, 9, 1490. DOI: 10.3390/mi13091490.
7. Castillo, O.; Castro, J. R.; Melin, P. Interval type-3 fuzzy control for automated tuning of image quality in televisions. *Axioms* **2022**, 11, 6, 276. DOI: 10.3390/axioms11060276.
8. Castillo, O.; Castro, J. R.; Melin, P. Forecasting the COVID-19 with interval type-3 fuzzy logic and the fractal dimension. *Int. J. Fuzzy Syst.* **2022**, 37, 10, 7909-7943. DOI: 10.1007/s40815-022-01351-7.
9. Castillo, O.; Castro, J. R.; Melin, P. A methodology for building interval type-3 fuzzy systems based on the principle of justifiable granularity. *Int. J. Intell. Syst.* **2022**, DOI:10.1002/int.22910.
10. Castillo, O.; Pulido, M.; Melin, P. Interval Type-3 Fuzzy Aggregators for Ensembles of Neural Networks in Time Series Prediction, In International Conference on Intelligent and Fuzzy Systems, Izmir, Turkey, Springer, Cham, pp. 785-793, 2022, DOI: 10.1007/978-3-031-09173-5-90.
11. Castillo, O.; Castro, J.R.; Melin, P. Interval type-3 fuzzy aggregation of neural networks for multiple time series prediction: the case of financial forecasting. *Axioms* **2022**, 11, 6. DOI; 10.3390/axioms11060251.
12. Castillo, O.; Castro, J. R.; Pulido, M.; Melin, P. Interval type-3 fuzzy aggregators for ensembles of neural networks in COVID-19 time series prediction. *Eng. Appl. Artif. Intel.* **2022**, 114, 105-110. DOI: 10.1016/j.engappai.2022.105110.
13. Mohammadzadeh, A.; Castillo, O.; Band, S. S.; Mosavi, A. A novel fractional-order multiple-model type-3 fuzzy control for nonlinear systems with unmodeled dynamics. *Int. J. Fuzzy Syst.* **2021**, 23, 6, 1633-1651. DOI: 10.1007/s40815-021-01058-1.

Preprints (www.preprints.org) | NOT PEER-REVIEWED | Posted: 31 October 2023 doi:10.20944/preprints202310.2072.v1

14. Aly, A.A.; Felemban, B.F.; Mohammadzadeh, V.; Castillo, O.; Bartoszewicz, A. Frequency regulation system: a deep learning identification, type-3 fuzzy control and LMI stability analysis. *Energies* **2021**, 14, 22, 7801. DOI: 10.3390/en14227801.
15. Castillo, O.; Valdez, F.; Peraza, C.; Yoon, J.H.; Geem, Z.W. High-speed interval type-2 fuzzy systems for dynamic parameter adaptation in harmony search for optimal design of fuzzy controllers. *Mathematics* **2021**, 9, 7, 758. DOI: 10.3390/math9070758.
16. Melin, P.; Sánchez, D.; Castro, J.R.; Castillo, O. Design of type-3 fuzzy systems and ensemble neural networks for COVID-19 time series prediction using a firefly algorithm. *Axioms* **2022**, 11, 8, 410. DOI: 10.3390/axioms11080410.
17. Kreinovich, V.; Kosheleva, O.; Melin, P.; Castillo, O. Efficient algorithms for data processing under type-3 (and higher) fuzzy uncertainty. *Mathematics* **2022**, 10, 13, 2361. DOI: 10.3390/math10132361.
18. Liu, Z.; Mohammadzadeh, A.; Turabieh, H.; Mafarja, M.; Band, S.; Mosavi, A. A new online learned interval type-3 fuzzy control system for solar energy management systems. *IEEE Access* **2021**, 9, 10498-10508. DOI: 10.1109/ACCESS.2021.3049301.
19. Mohammadzadeh, A.; Sabzalian, M.H.; Zhang, W. An interval type-3 fuzzy system and a new online fractional-order learning algorithm: theory and practice. *IEEE T. Fuzzy Syst.* **2019**, 28, 9, 1940-1950. DOI: 10.1109/TFUZZ.2019.2928509.
20. Tian, M. W.; Yan, S. R.; Mohammadzadeh, A.; Tavoosi, J.; Mobayen, S.; Safdar, R.; Assawinchaichote, W.; Vu, M. A.; Zhilenkov, A. Stability of interval type-3 fuzzy controllers for autonomous vehicles. *Mathematics* **2021**, 9, 21, 2742. DOI: 10.3390/math9212742.
21. Taghieh, A.; Mohammadzadeh, C.; Zhang, S.; Rathinasamy; Bekiros, S. A novel adaptive interval type-3 neuro-fuzzy robust controller for nonlinear complex dynamical systems with inherent uncertainties. *Nonlinear Dyn.* **2022**, 1-15. DOI: 10.1007/s11071-022-07867-9.
22. Singh, D. J.; Verma, N. K.; Ghosh, A. K.; Malagaudanavar, A. An approach towards the design of interval type-3 T-S fuzzy system. *IEEE T. Fuzzy Syst.* **2022**, 30, 9, 3880-3893. DOI: 10.1109/TFUZZ.2021.3133083.
23. Gheisarnejad, M.; Mohammadzadeh, A.; Khooban, M. H. Model predictive control-based type-3 fuzzy estimator for voltage stabilization of DC power converters. *IEEE T. Ind. Electron.* **2021**, 69, 12, 13849-13858. DOI: 10.1109/TIE.2021.3134052.
24. Qasem, S.N.; Ahmadian, A.; Mohammadzadeh, A.; Rathinasamy, S.; Pahlevanzadeh, B. A type-3 logic fuzzy system: optimized by a correntropy based Kalman filter with adaptive fuzzy kernel size. *Inf Sci* **2021**, 572, 424-443. DOI: 10.1016/j.ins.2021.05.031.
25. Gheisarnejad, M.; Mohammadzadeh, A.; Farsizadeh,V.; Khooban, M.H. Stabilization of 5G telecom converter-based deep type-3 fuzzy machine learning control for telecom applications. *IEEE T. Circuits-II* **2021**, 69, 544-548. DOI: 10.1109/TCSII.2021.3102282.
26. Taghieh, A.; Mohammadzadeh, A.; Zhang, C.; Kausar, N.; Castillo, O. A type-3 fuzzy control for current sharing and voltage balancing in microgrids. *Appl. Soft Comput.* **2022**, 129,109636. DOI: 10.1016/j.asoc.2022.109636.
27. Taghieh, A.; Zhang, C.; Alattas, K. A.; Bouteraa, Y.; Rathinasamy, S.; Mohammadzadeh, A. A predictive type-3 fuzzy control for underactuated surface vehicles. *Ocean Eng.* **2022**, 266, 11301. DOI: 10.1016/j.oceaneng.2022.113014.
28. Wang, J. H.; Tavoosi, J.; Mohammadzadeh, A.; Mobayen, S.; Asad, J. H.; Assawinchaichote, W.; Vu, M. T-.; Skruch, P. Non-Singleton type-3 fuzzy approach for flowmeter fault detection, experimental study in a gas industry. *Sensors* **2021**, 21, 21, 7419. DOI: 10.3390/s21217419.
29. Balootaki, M. A.; Rahmani, H.; Moeinkhah, H.; Mohammadzadeh, A. Non-singleton fuzzy control for multisynchronization of chaotic systems. *Appl. Soft Comput.* **2020**, 99, 4, 106924. DOI: 10.1016/j.asoc.2020.106924.
30. Alattas, K.A.; Mohammadzadeh, A.; Mobayen, S.; Aly, A.A.; Felemban, B.F. A new data-driven control system for MEMSs gyroscopes: dynamics estimation by type-3 fuzzy systems. *Micromachines* **2021**, 12, 11, 1390. DOI: 10.3390/mi12111390.
31. Mosavi, A.; Shokri, S.N.; Qasem, M.; Band, S.S.; Mohammadzadeh, A. Fractional-order fuzzy control approach for photovoltaic/battery systems under unknown dynamics, variable irradiation and temperature. *Electronics* **2020**, 9, 9, 1455. DOI: 10.3390/electronics9091455.
32. Tian, M.W.; Mohammadzadeh, A.; Tavoosi, J.; Mobayen, S.; Asad, J.H.; Castillo, O.; Várkonyi-Kóczy, A.R. A deep-learned type-3 fuzzy system and its application in modeling problems. *Acta Polytechnica Hungarica* **2022**, 19, 2, 151-172. DOI: 10.1016/j.egyr.2021.07.004.
33. Tian, M.W.; Bouteraa, Y.; Alattas, K.A.; Yan, S.R.; Alanazi, A.K.; Mohammadzadeh, A.; Mobayen, S. A type-3 fuzzy approach for stabilization and synchronization of chaotic systems: applicable for financial and physical chaotic systems. *Complexity* **2022**. DOI: 10.1155/2022/8437910.
34. Mohammadzadeh, A.; Vafaie, R.H. A deep learned fuzzy control for inertial sensing: micro electromechanical systems. *Appl. Soft Comput.* **2021**, 109. DOI: 10.1016/j.asoc.2021.107597.

Preprints (www.preprints.org) | NOT PEER-REVIEWED | Posted: 31 October 2023 doi:10.20944/preprints202310.2072.v1

35. Nabipour, N.; Qasem, S.N.; Jermsittiparsert, K. Type-3 fuzzy voltage management in PV/hydrogen fuel cell/battery hybrid systems. *Int. J. Hydrogen Energ.* **2020**, 45, 56, 32478-32492. DOI: 10.1016/j.ijhydene.2020.08.261.
36. Hua, G.; Wang, F.; Zhang, J.; Alattas, K.A.; Mohammadzadeh, A.; The Vu, M. A new type-3 fuzzy predictive approach for mobile robots. *Mathematics* 2021, 10, 17, 3186. DOI: 0.3390/math10173186.
37. Yan, S.; Aly, A.A.; Felemban, B.F.; Gheisarnejad, M.; Tian, M.; Khooban, M.H.; Mohammadzadeh, A.; Mobayen, S. A new event-triggered type-3 fuzzy control system for multi-agent systems: optimal economic efficient approach for actuator activating. *Electronics* **2021**, 10, 24, 3122, 2021. DOI: 10.3390/electronics10243122.
38. Cao, Y.; Raise, A.; Mohammadzadeh, A.; Rathinasamy, S.; Band, S.S.; Mosavi, A. Deep learned recurrent type-3 fuzzy system: applications for renewable energy modeling/prediction. *Energy Reports* **2021**, 7, 8115-8127. DOI: 10.1016/j.egyr.2021.07.004.
39. Ma, C.; Mohammadzadeh, A.; Turabieh, H.; Mafarja, M.; Band, S. S.; Mosavi, A. Optimal type-3 fuzzy system for solving singular multi-pantograph equations. *IEEE Access* **2020**, 8, 225692-225702. DOI: 10.1109/ACCESS.2020.3044548.
40. Vafaie, R.H.; A. Mohammadzadeh, A.; Piran, M.J. A new type-3 fuzzy predictive controller for mems gyroscopes. *Nonlinear Dynam.* **2021**, 106, 381-403. DOI: 10.1007/s11071-021-06830-4.
41. Montes-Dorantes, P.N.; Méndez, G.M. Non-Iterative Wagner-Hagras General type-2 Mamdani Singleton Fuzzy logic System Optimized by Central Composite Design in Quality Assurance by Image Processing. In: Castillo O., Kumar A. (eds) Recent trends on Type-2 Fuzzy Logic Systems: Theory, Methodology and Applications, Studies in Fuzziness and Soft Computing 425. 2023. DOI 10.1007/978-3-031-26332-3_13.
42. Melin, P.; Castillo, O. An intelligent hybrid approach for industrial quality control combining neural networks, fuzzy logic, and fractal theory. Inf. Sci. **2007**, 177, 1543-1557.
43. Gilan, S.S.; Sebt, M.H.; Shahhosseini, V. Computing with words for hierarchical competency-based selection of personnel in construction companies. *Appl. Soft Comput.* **2012**, 12, 860-871.
44. Shahparast, H.; Mansoori, E.G. Developing an online general type-2 fuzzy classifier using evolving type-1 rules. *Int. J. Approx. Reason.* **2019**, 113, 336-353.
45. Cheng-Dong, L.I.; Gui-Qing, Z.; Hui-Dong, W.; Wei-Na, R. Properties and data-driven design of perceptual reasoning method based linguistic dynamic systems. *Acta Autom. Sin.* **2014**, 40, 2221-2232.
46. Mittal, K.; Jain, A.; Vaisla, K.S.; Castillo, O.; Kacprzyk, J. A comprehensive review on type 2 fuzzy logic applications: Past, present and future. *Eng. Appl. Artif. Intell.* **2020**, 95, 103916.
47. Ibrahim, A.A.; Zhou, H.B.; Tan, S.X.; Zhang, C.L.; Duan, J.A. Regulated Kalman filter based training of an interval type-2 fuzzy system and its evaluation. *Eng. Appl. Artif. Intell.* **2020**, 95, 103867.
48. Balootaki, M.A.; Rahmani, H.; Moeinkhah, H.; Mohammadzadeh, A. On the synchronization and stabilization of fractional-order chaotic systems: Recent advances and future perspectives. *Physica A: Statistical Mechanics and its Applications* **2020**, 551, 124203.
49. Ontiveros, E.; Melin P.; Castillo, O. High order $\boldsymbol{\alpha}$-planes integration: A new approach to computational cost reduction of General Type-2 Fuzzy Systems. *Eng. Appl. Artif. Intell.* **2018**, 4, 186–197.
50. Wu, D.; Mendel, J.M. Recommendations on designing practical interval type-2 fuzzy systems. *Eng. Appl. Artif. Intell.* **2019**, 85, 182-193.
51. Chiclana F. & Zhou S. M. Type-reduction of general type-2 fuzzy sets: the type-1 OWA approach. *Int. J. Intell. Syst.* **2013**, 28, 505-522.
52. Jeng, W.H.R.; Yeh, C.Y.; Lee, S. J. General Type-2 Fuzzy Neural Network with Hybrid Learning for Function Approximation. In 2009 IEEE International Conference on Fuzzy Systems, Jeju, Korea (South), pp. 1534-1539, 2009.
53. Figueroa-García, J.C.; Román-Flores, H.; Chalco-Cano, Y. Type–reduction of interval type–2 fuzzy numbers via the Chebyshev inequality. *Fuzzy Sets Syst.* **2022**, 435, 164-180.
54. Yu, Q.; Dian, S.; Li, Y.; Liu, J.; Zhao, T. Similarity-based non-singleton general type-2 fuzzy logic controller with applications to mobile two-wheeled robots. *J. Intell. Fuzzy Syst.* **2019**, 37, 5, 6841-6854. https://doi.org/10.3233/JIFS-190683.
55. Zhao, T.; Yu, Q.; Dian, S.; Guo, R.; Li, S. Non-singleton general type-2 fuzzy control for a two-wheeled self-balancing robot. *Int. J. Fuzzy Syst.* **2019**, 21, 6, 1724-1737. https://doi.org/10.1007/s40815-019-00664-4.
56. Y Chen, Y.; Wang, D. Forecasting by general type-2 fuzzy logic systems optimized with QPSO algorithms. *Int. J. Control Autom. Syst.* **2017**, 15, 6, 2950-2958. https://doi.org/10.1007/s12555-017-0793-0.
57. Li, X.; Chen, Y. Discrete non-iterative centroid type-reduction algorithms on general type-2 fuzzy logic systems. *Int. J. Fuzzy Syst.* **2021**, 23, 3, 704-715. https://doi.org/10.1007/s40815-020-00996-6.
58. Zhao, T.; Liu, J.; Dian, S.; Guo, R.; Li, S. Sliding-mode-control-theory-based adaptive general type-2 fuzzy neural network control for power-line inspection robots. *Neurocomputing* **2020**, 401, 281-294. https://doi.org/10.1016/j.neucom.2020.03.050.
59. Mai, D.S.; Dang, T.H.; Ngo, L.T. Optimization of interval type-2 fuzzy system using the PSO technique for predictive problems. *J. Inf. Telecommun.* **2021**, 5, 2, 197-213. https://doi.org/10.1080/24751839.2020.1833141.

Preprints (www.preprints.org) | NOT PEER-REVIEWED | Posted: 31 October 2023 doi:10.20944/preprints202310.2072.v1

60. Mohammadzadeh, A.; Kumbasar, T. A new fractional-order general type-2 fuzzy predictive control system and its application for glucose level regulation. *Appl. Soft Comp.* **2020**, 91, 106241. https://doi.org/10.1016/j.asoc.2020.106241.
61. Mohammadzadeh, A.; Ghaemi, S.; Kaynak, O.; Khanmohammadi, S. Observer-based method for synchronization of uncertain fractional order chaotic systems by the use of a general type-2 fuzzy system. *App Soft Comp.* **2016**, 49, 544-560. https://doi.org/10.1016/j.asoc.2016.08.016.
62. Figueroa-García, J.C.; Román-Flores, H.; Chalco-Cano, Y. Type–reduction of interval type–2 fuzzy numbers via the chebyshev inequality. *Fuzzy Sets Syst.* **2021**, 435; pp. 164-180. https://doi.org/10.1016/j.fss.2021.04.014.
63. Geramian, A.; Abraham, A. Customer classification: a mamdani fuzzy inference system standpoint for modifying the failure mode and effect analysis based three-dimensional approach. *Expert Syst. Appl.* **2021**, 186, 115753. https://doi.org/10.1016/j.eswa.2021.115753.
64. Tavana, M.R.; Khooban, M.H.; Niknam, T. Adaptive PI controller to voltage regulation in power systems: STATCOM as a case study. *ISA Trans.* **2017**, 66, 325-334. https://doi.org/10.1016/j.isatra.2016.09.027.
65. Mohammadzadeh, A.; Sabzalian, M.H.; Ahmadian, A.; Nabipour, N. A dynamic general type-2 fuzzy system with optimized secondary membership for online frequency regulation. *ISA Trans.* **2021**, 112, 150-160. https://doi.org/10.1016/j.isatra.2020.12.008.
66. Torshizi, A.D.; Zarandi, M.H.F. A new cluster validity measure based on general type-2 fuzzy sets: application in gene expression data clustering. *Knowl. Based Syst.* **2014**, 64, 81-93. https://doi.org/10.1016/j.knosys.2014.03.023.
67. Khooban, M.H.; Vafamand, N.; Liaghat, A.; Dragicevic, T. An optimal general type-2 fuzzy controller for urban traffic network. *ISA Trans.* **2017**, 66, 335-343. https://doi.org/10.1016/j.isatra.2016.10.011
68. Mohammadzadeh, A.; Kaynak, O. A novel general type-2 fuzzy controller for fractional-order multi-agent systems under unknown time-varying topology. *J. Franklin Inst.* 2019, 356, 5151-5171. https://doi.org/10.1016/j.jfranklin.2019.05.006
69. Ontiveros, E.; Melin, P.; Castillo, O. Comparative study of interval type-2 and general type-2 fuzzy systems in medical diagnosis. *Inf. Sci.* **2020**, 525, 37-53. https://doi.org/10.1016/j.ins.2020.03.059.
70. Zarandi, M.F.; Soltanzadeh, S.; Mohammadi, A.; Castillo, O. Designing a general type-2 fuzzy expert system for diagnosis of depression. *Appl. Soft Comput*. **2019**, 80, 329-341. https://doi.org/10.1016/j.asoc.2019.03.027.
71. Salehi, F.; Keyvanpour, M.R.; Sharifi, A. GT2-CFC: General type-2 collaborative fuzzy clustering method. *Inf. Sci*. **2021**, 578, 297-322. https://doi.org/10.1016/j.ins.2021.07.037.
72. Almaraashi, M.; John, R.; Hopgood, A.; Ahmadi, S. Learning of interval and general type-2 fuzzy logic systems using simulated annealing: Theory and practice. *Inf. Sci.* **2016**, 360, 21-42. https://doi.org/10.1016/j.ins.2016.03.047.
73. Carvajal, O.; Melin, P.; Miramontes, I.; Prado-Arechiga, G. Optimal design of a general type-2 fuzzy classifier for the pulse level and its hardware implementation. *Eng. Appl. Artif. Intel.* **2021**, 97, 104069. https://doi.org/10.1016/j.engappai.2020.104069.
74. Ontiveros-Robles, E.; Castillo, O.; Melin, P. Towards asymmetric uncertainty modeling in designing general type-2 fuzzy classifiers for medical diagnosis. *Expert Syst. Appl.* **2021**, 183, 115370. https://doi.org/10.1016/j.eswa.2021.115370.
75. Doctor, F.; Syue, C.H.; Liu, Y.X.; Shieh, J. S.; Iqbal, R. Type-2 fuzzy sets applied to multivariable self-organizing fuzzy logic controllers for regulating anesthesia. *Appl. Soft Comput*. **2016**, 38, 872-889. https://doi.org/10.1016/j.asoc.2015.10.014.
76. Castillo, O.; Muhuri, P.K.; Melin, P.; Pulkkinen, P. Emerging issues and applications of type-2 fuzzy sets and systems. *Eng. Appl. Artif. Intel.* **2020**, 90, 103596. https://doi.org/10.1016/j.engappai.2020.103596.
77. Sahab, N.; Hagras, H. Adaptive non-singleton type-2 fuzzy logic systems: A way forward for handling numerical uncertainties in real world applications. *Int. J. Comput. Commun. Control* **2011**, 6, 503-529.
78. Ontiveros-Robles, E.; Melin, P. A hybrid design of shadowed type-2 fuzzy inference systems applied in diagnosis problems. *Eng. Appl. Artif. Intel.* **2019**, 86, 43-55. https://doi.org/10.1016/j.engappai.2019.08.017.
79. Ochoa, P.; Castillo, O.; Melin, P.; Soria, J. Differential evolution with shadowed and general type-2 fuzzy systems for dynamic parameter adaptation in optimal design of fuzzy controllers. *Axioms* **2021**, 10, 3, 194. https://doi.org/10.3390/axioms10030194.
80. Wagner, C.; Hagras, H. Toward general type-2 fuzzy logic systems based on zSlices. *IEEE Trans. Fuzzy Syst.* **2010**, 18, 637-660. https://doi.org 10.1109/TFUZZ.2010.2045386.
81. Shi, J.; Song, Y. Mathematical analysis of a simplified general type-2 fuzzy PID controller. *Math. Biosci. Eng.* **2020**, 17, 6, 7994-8036. https://doi.org/10.3934/mbe.2020406.
82. Ontiveros-Robles, E.; Melin, P.; Castillo, O. An efficient high-order α-plane aggregation in general type-2 fuzzy systems using newton–cotes rules. *Int. J. Fuzzy Syst.* **2021**, 23, 1102-1121. https://doi.org/10.1007/s40815-020-01031-4.

Preprints (www.preprints.org) | NOT PEER-REVIEWED | Posted: 31 October 2023 doi:10.20944/preprints202310.2072.v1

83. Melin, P.; Ontiveros-Robles, E.; Castillo, O. New Medical Diagnosis Models Based on Generalized Type-2 Fuzzy Logic. 1st ed. Springer International Publishing. 2021. https://doi.org/10.1007/978-3-030-75097-8.
84. Chen, Y.; Li, C.; Yang, J. Design and application of Nagar-Bardini structure-based interval type-2 fuzzy logic systems optimized with the combination of backpropagation algorithms and recursive least square algorithms. *Expert Syst Appl* **2023**, 211, 118596. https://doi.org/10.1016/j.eswa.2022.118596.
85. El-Nagar, A.M.; El-Bardini, M.; Khater, A.A. A class of general type-2 fuzzy controller based on adaptive alpha-plane for nonlinear systems. *Appl. Soft Comput.* **2023**, 133, 109938. https://doi.org/10.1016/j.asoc.2022.109938.
86. Hazarika, B.B.; Gupta, D. Affinity based fuzzy kernel ridge regression classifier for binary class imbalance learning. *Eng. Appl. Artif. Intel.* **2023**, 117, 105544. https://doi.org/10.1016/j.engappai.2022.105544.
87. Yin, R.; Pan, X.; Zhang, L.; Yang, J.; Lu, W. A rule-based deep fuzzy system with nonlinear fuzzy feature transform for data classification. *Inf Sci* **2023**, 633, 431-452. https://doi.org/10.1016/j.ins.2023.03.071.
88. Sabahi, K.; Zhang, C.; Kausar, N.; Mohammadzadeh, A.; Pamucar, D.; Mosavi, A.H. Input-output scaling factors tuning of type-2 fuzzy PID controller using multi-objective optimization technique. *AIMS Mathematics* **2022**, 8, 4, 7917-7932. https://doi.org /10.3934/math.2023399.
89. Sedaghati, A.; Pariz, N.; Siahi, M.; Barzamini, R. A new adaptive non-singleton general type-2 fuzzy control of induction motors subject to unknown time-varying dynamics and unknown load torque. *Soft Comput*. **2021**, 25, 5895-5907. https://doi.org/10.1007/s00500-021-05582-y.
90. Sabzalian, M.H.; Mohammadzadeh, A.; Rathinasamy, S.; Zhang, W. A developed observer-based type-2 fuzzy control for chaotic systems. Int. J. Syst. Sci. **2021**, 1-20. https://doi.org/10.1080/00207721.2021.1918282.
91. Huang, H.; Xu, H.; Chen, F.; Zhang, C.; Mohammadzadeh, A. An applied type-3 fuzzy logic system: practical matlab simulink and M-files for robotic, control, and modeling applications. *Symmetry* **2023**, 15, 2, 475.
92. Mehrmolaei, S.; Savargiv, M.; Keyvanpour, M.R. (2023). Hybrid learning-oriented approaches for predicting Covid-19 time series data: A comparative analytical study. *Eng. Appl. Artif. Intell.* **2023**, 126, 106754
93. Elhaki, O.; Shojaei, K.; Mohammadzadeh, A.; Rathinasamy, S. Robust amplitude-limited interval type-3 neuro-fuzzy controller for robot manipulators with prescribed performance by output feedback. *Neural Comput. Appl.* **2023**, 35, 12, 9115-9130.
94. Castillo, O.; Castro, J.R.; Melin, P. Interval Type-3 Fuzzy Systems: A Natural Evolution from Type-1 and Type-2 Fuzzy Systems. In *Fuzzy Logic and Neural Networks for Hybrid Intelligent System Design*, Cham: Springer International Publishing. 2023; pp. 209-221.
95. Yan, B.; Jiang, X.; Alattas, K.A.; Zhang, C.; Mohammadzadeh, A. Generation of limit cycles in nonlinear systems: Machine leaning based type-3 fuzzy control. *IEEE Access* **2023**.
96. Vinothkumar, J.; Thamizhselvan, D. Enhancing controller efficiency in hybrid power system using interval type 3 fuzzy controller with bacterial foraging optimization algorithm. *J. Theor. Appl. Inf. Technol.* **2023**, 101, 12.
97. Tarafdar, A.; Majumder, P.; Deb, M.; Bera, U.K. Application of a q-rung orthopair hesitant fuzzy aggregated Type-3 fuzzy logic in the characterization of performance-emission profile of a single cylinder CI-engine operating with hydrogen in dual fuel mode. *Energy* **2023**, 269, 126751.
98. Tarafdar, A.; Majumder, P.; Deb, M.; Bera, U. K. Performance-emission optimization in a single cylinder CI-engine with diesel hydrogen dual fuel: A spherical fuzzy MARCOS MCGDM based Type-3 fuzzy logic approach. *Int. J. Hydrogen Energ.* **2023**.
99. SINGH, D.; Verma, N. Interval Type-3 TS Fuzzy System for Nonlinear Aerodynamic Modelling. *Available at SSRN 4428696*.
100. Elhaki, O.; Shojaei, K.; Mohammadzadeh, A. Robust state and output feedback prescribed performance interval type-3 fuzzy reinforcement learning controller for an unmanned aerial vehicle with actuator saturation. *IET Control Theory A.* **2023**, 17, 5, 605-627.
101. Yildirim, B.; Gheisarnejad, M.; Mohammadzadeh, A.; Khooban, M.H. Intelligent frequency stabilization of low-inertia islanded power grids-based redox battery. *J. Energy Storage* **2023**, 71, 108190.
102. Cuevas, F.; Castillo, O.; Cortés-Antonio, P. Generalized type-2 fuzzy parameter adaptation in the marine predator algorithm for fuzzy controller parameterization in mobile robots. *Symmetry* **2022**, 14, 5, 859.
103. Yahiaoui, F.; Chabour, F.; Guenounou, O.; Bajaj, M.; Hussain-Bukhari, S.S.; Shahzad-Nazir, M.; Mbadjoun-Wapet, D.E. An experimental testing of optimized fuzzy logic-based MPPT for a standalone PV system using genetic algorithms. *Mat. Probl. Eng.* ***2023***.
104. Ochoa, P.; Castillo, O.; Melin, P.; Castro, J.R. Interval type-3 fuzzy differential evolution for parameterization of fuzzy controllers. *Int. J. Fuzzy Syst.* ***2023***, 1360-1376.
105. Peraza, C.; Castillo, O.; Melin, P.; Castro, J.R.; Yoon, J.H.; Geem, Z.W. A type-3 fuzzy parameter adjustment in harmony search for the parameterization of fuzzy controllers. *Int. J. Fuzzy Syst.* **2023**, 25, 2281-2294.

Preprints (www.preprints.org) | NOT PEER-REVIEWED | Posted: 31 October 2023 doi:10.20944/preprints202310.2072.v1

106. Castillo, O.; Peraza, C.; Ochoa, P.; Amador-Angulo, L.; Melin, P.; Park, Y.; Geem, Z. W. Shadowed type-2 fuzzy systems for dynamic parameter adaptation in harmony search and differential evolution for optimal design of fuzzy controllers. *Mathematics* **2021**, 9, 19, 2439.
107. Amador-Angulo, L.; Castillo, O.; Castro, J.R.; Melin, P. A new approach for interval type-3 fuzzy control of nonlinear plants. *Int. J. Fuzzy Syst.* **2023**, 1-19.
108. Bie, H., Li, P., Chen, F., Ghaderpour, E. An observer-based type-3 fuzzy control for non-holonomic wheeled robots. *Symmetry* ***2023***, 15, 7, 1354.
109. Yunjun, C.; Chao, J.; Jiuzhi, D.; Zhanshan, Z. Output feedback sliding mode control based on adaptive sliding mode disturbance observer. *Meas. Control* **2022**. 55, 7-8, 646-656.
110. Li, H.; Dai, X.; Zhou, L.; Wu, Q. Encoding words into interval type-2 fuzzy sets: The retained region approach. *Inf. Sci.* **2023,** 629, 760-777.
111. Abid, M.S.; Apon, H.J.; Nafi, I.M.; Ahmed, A.; Ahshan, R. Multi-objective architecture for strategic integration of distributed energy resources and battery storage system in microgrids. *J. Energy Storage* **2023**, 72, 108276.
112. Tarafdar, A.; Majumder, P.; Bera, U.K. Prediction of Air Quality Index in Kolkata City Using an Advanced Learned Interval Type-3 Fuzzy Logic System. In 2023 IEEE 8th International Conference for Convergence in Technology (I2CT), April 2023; pp. 1-7.
113. Rituraj, R.; Ecker, D.A. Comprehensive Investigation into the Application of Convolutional Neural Networks (ConvNet/CNN) in Smart Grids. In 2022 IEEE 22nd International Symposium on Computational Intelligence and Informatics and 8th IEEE International Conference on Recent Achievements in Mechatronics, Automation, Computer Science and Robotics (CINTI-MACRo), IEEE.Smart and Sustainable Grids Using Data-Driven Methods; Considering Artificial Neural Networks and Decision Trees, November 2022; pp. 000359-000368.
114. Luo, Q.; Bai, J.; Wu, F. Improved constrained predictive functional control using extended non-minimal state space formulation for the cement production process. *Processes* **2022**, 10, 5, 969.
115. Zhu, C.; Liu, R.; Li, B.; Xia, J.; Zhang, N. Neural network-based event-triggered adaptive asymptotic tracking control for switched nonlinear systems. *Int. J. Control Autom.* **2022**, 20, 6, 2021-2031.
116. Gao, P.; Zhang, H., Wu, Z.; Wang, J. Visualizing the expansion and spread of coronavirus disease 2019 by cartograms. *Environ. Plan. A: Economy and Space* **2000**, 52, 4, 698-701.
117. An explication of the 800-day COVID-19 pandemic spread behavior of seven countries from different continents and the world total in a non-linear time series framework. Available online: https://www.researchsquare.com/article/rs-2780972/v2 (accessed on 06 08 2023).
118. Mendez, G.M. Orthogonal-Back Propagation Hybrid Learning Algorithm for Type-2 Fuzzy Logic Systems, Proceedings of NAFIPS 04 IEEE International Conference on Fuzzy Sets, Banff, Alberta Canada, June 27-30-2004; pp. 899-902.
119. Mendez, G.M.; López-Juarez, I. Orthogonal-Back Propagation Hybrid Learning Algorithm for Interval Type-1 Non-Singleton Type-2 Fuzzy Logic Systems, WSEAS Transactions on Systems, Issue 3, Vol. 4, March 2005; pp. 212-218.
120. Mendez, G.M.; Medina, M.A. Orthogonal-Back Propagation Hybrid Learning Algorithm for Interval Type-2 Non-Singleton Type-2 Fuzzy Logic Systems., IASTED International Conference on Intelligent Systems and Control, Cambridge, MA, USA, October-November 2005; pp. 386-391.
121. Méndez, G.M.; Hernandez, M.A. Hybrid learning for interval type-2 fuzzy logic systems based on orthogonal least-squares and back-propagation methods. *Inf. Sci.* **2009**, 179, 13, 2146-2157.
122. Méndez, G.M.; Martinez, J.C.; González, D. S.; Rendón-Espinoza, F. J. Orthogonal-least-squares and backpropagation hybrid learning algorithm for interval A2-C1 singleton type-2 Takagi-Sugeno-Kang fuzzy logic systems. *Int. J. Hybrid Intell. Syst.* **2014,** 11, 2, 125-135.
123. Hernandez, M.A.; Melin, P.; Méndez, G.M.; Castillo, O.; López-Juarez, I. A hybrid learning method composed by the orthogonal least-squares and the back-propagation learning algorithms for interval A2-C1 type-1 non-singleton type-2 TSK fuzzy logic systems. *Soft. Comput.* **2015**, 19, 661-678.
124. Mendel, J.M. *Uncertain rule-based fuzzy systems. Introduction and new directions*, 2nd ed.; Springer: Cham, Switzerland, 2017, DOI: 10.1007/978-3-319-51370-6.
125. Aguado, A. *Temas de Identificación y Control Adaptable*; Instituto de Cibernética, Matemática y Física, 1rst ed. Cuba, 2000.
126. Mendez, G.M.; Leduc, L.A.; Colas, R.; Cavazos, A.; Soto, R. Modelling recalescence after stock reduction during hot strip rolling,", *Ironmak. Steelmak.* **2013**, 33, 6, 484-492. DOI: 10.1179/174328106X114011.

Disclaimer/Publisher's Note: The statements, opinions and data contained in all publications are solely those of the individual author(s) and contributor(s) and not of MDPI and/or the editor(s). MDPI and/or the editor(s) disclaim responsibility for any injury to people or property resulting from any ideas, methods, instructions or products referred to in the content.